NPS ARCHIVE
1962
CHRISTY, R.

PRINCETON UNIVERSITY

TMENT OF AERONAUTICAL ENGINEERING

Thesis
C478

DUDLEY KNOX LIBRARY
NAVAL POSTGRADUATE SCHOOL
MONTEREY CA 93943-5101

AN INVESTIGATION OF THE LONGITUDINAL STATIC STABILITY OF AN AUTOGYRO

Robert A. Christy

Aeronautical Engineering Report No. 610

May 1962

Submitted in partial fulfillment of the requirements for the degree of Master of Science in Engineering from Princeton University, 1962.

DUDLEY KNOX LIBRARY
NAVAL POSTGRADUATE SCHOOL
MONTEREY CA 93943-5101

ACKNOWLEDGEMENTS

The author wishes to gratefully acknowledge the guidance and assistance of the Faculty of the Aeronautical Engineering Department of Princeton University, to Prof. Edward Seckel, Prof. A. A. Nikolsky, and Research Associate H. C. Curtiss, Jr., in particular. Further, the kind indulgence of the Department for facilities for the test aircraft and invaluable assistance of the several maintenance personnel are gratefully acknowledged.

TABLE OF CONTENTS

	Acknowledgements	i
	Table of Contents	ii
	List of Figures	iii
	List of Symbols and Nomenclature	iv
	Summary	vii
I.	INTRODUCTION	1
II.	ANALYSIS	5
III.	EQUIPMENT AND PROCEDURE	20
IV.	RESULTS AND DISCUSSION	25
V.	CONCLUSIONS	33
VI.	REFERENCES	34
	Figures	35
	APPENDIX I - Physical Constants	58
	APPENDIX II - Torque Relations	59

LIST OF FIGURES

Figure

1. Photograph of the test aircraft
2. Sketch of axis system
3. Plot of λ versus μ
4. Plot of $\left.\frac{\partial \Omega}{\partial v}\right|_{\alpha}$ versus μ
5. Plot of $\left.\frac{\partial \Omega}{\partial \alpha}\right|_{v}$ versus μ
6. Plot of Z_v versus μ
7. Plot of Z_α versus μ
8. Plot of C_T, C_H versus μ
9. Plot of H versus μ
10. Plot of H_v versus μ
11. Plot of H_α versus μ
12. Plot of fuselage and power contributions to stability versus μ
13. Plot of $(M_v)_{rotor}$ versus μ
14. Plot of $(M_\alpha)_{rotor}$ versus μ
15. Plot of M_v versus μ
16. Plot of M_α versus μ
17. Plot of M_δ versus μ
18. Airspeed calibration curve
19. Rotor blade section characteristics
20. Flight test trim curve δ versus v
21. Flight test trim curve α_1 versus v
22. Flight test trim curve α versus v
23. Plot of static stability E versus μ

LIST OF FIGURES AND NOMENCLATURE

B	Rotor tip loss factor. Taken as $B = 1 - \frac{c}{\Omega R}$	n.d.
C_H	Rotor H Force coefficient, $C_H = \frac{H}{\rho \pi R^2 (\Omega R)^2}$	n.d.
C_Q	Rotor Torque coefficient, $C_Q = \frac{Q}{\rho \pi R^3 (\Omega R)^2}$	n.d.
C_T	Rotor Thrust coefficient, $C_T = \frac{T}{\rho \pi R^2 (\Omega R)^2}$	n.d.
D_f	Fuselage drag	lbs.
E	Coefficient of constant term in the characteristic or frequency equation. A measure of static stability.	n.d.
F	Generalized force	lbs.
H	Rotor horizontal force, the longitudinal projection of the rotor resultant force vector into the plane perpendicular to the axis of no feathering, positive aft.	lbs.
I_1	Mass moment of inertia of rotor blade about flapping hinge	slug ft^2
K_I	Non-dimensionalizing term $K_I = \rho \pi R^2 (\Omega R)^2$	lbs.
M	Longitudinal pitching moment about the c.g. of the aircraft, positive nose up.	ft lbs.
M_{f_p}	Longitudinal pitching moment due to fuselage and power effects	ft lbs.
M_V, M_α	Generalized pitching moment derivatives	
N_p	Normal force due to thrusting propeller, positive up	lbs.
Q	Shaft torque	
R	Main rotor radius	ft.
S_t	Area of horizontal tail surface	ft^2

T	Rotor thrust, projection of rotor' result nt force vector upon the axis of no feathering	l b.
T_p	Thrust of engine-propeller, positive forward	l b.
V	Magnitude of forward velocity projected upon the X axis	ft/sec
W	Gross weight of the aircraft	l b.
X,Y,Z	Stability axis, a body axis that is initially oriented with the relative velocity vector and fixed in the aircraft after zero time. X is positive forward, Z is positive down. Origin at c.g. of aircraft.	
Z_V, Z_α	Generalized force derivatives in Z direction	
a	Lift curve slope of rotor blade section	l/radian
a_o	Rotor coning angle	radians
a_1	Longitudinal angle between the axis of no feathering and the axis of no flapping, positive for flapping axis aft	radians
a_t	Three-dimensional lift curve slope of horizontal tail	l/radian
b	Number of blades of main rotor	
b_1	Lateral angle between axis of no feathering and axis of no flapping, positive for flapping axis right	radians
c	Rotor blade chord	ft.
c.g.	Center of gravity of aircraft	
i_R	Incidence of rotor reference axis relative to fuselage reference axis	radians
q	Free stream dynamic pressure	l /ft^2
v	Average induced velocity at the rotor disc	ft/sec
$\bar{x},\bar{z}$	Displacement of rotor hub from aircraft c.g., measured perpendicular to and along rotor reference axis. Negative for rotor hub above and aft of c.g.	ft.

x_p, z_p	Displacement of engine-propeller thrust axis from aircraft c.g. Measured along stability axes	ft.
x_t	Tail arm, measured along stability axes	ft.
α	Angle of attack of the plane of no feathering, positive up	radians
α_f	Angle of attack of the fuselage reference line	radians
α_p	Angle of attack of the thrusting propeller, equal to fuselage angle of attack	radians
α_t	Angle of attack horizontal tail, equal to fuselage angle of attack	radians
α_1	Angle of attack of the plane perpendicular to the rotor reference axis	radians
γ	Flight path angle	radians
γ_1	Blade constant, $\gamma_1 = \frac{\rho a c R^4}{I_1}$	n.d.
Δ	Increment or incremental change	n.d.
δ	Rotor control angle, the longitudinal angle between the rotor reference axis and axis of no feathering, positive for axis of no feathering, aft	radians
$\bar{\delta}$	Mean blade profile drag coefficient	n.d.
	Instantaneous rotor blade pitch angle	radians
λ	Inflow ratio, $\lambda = \frac{V\sin\alpha - v}{\Omega R}$	n.d.
μ	Tip speed ratio, $\mu = \frac{V\cos\alpha}{\Omega R}$	n.d.
ρ	Mass density of the air	slugs/ft^3
σ	Rotor solidity $\sigma = \frac{bc}{\pi R}$	n.d.
Ω	Rotor angular velocity	rad/sec

To indicate that rotor speed is a variable in accordance with torque equilibrium derivatives so taken are designated with $\Big|_{Q=0}$. Derivatives taken with rotor speed specifically held constant will be designated with $\Big|_{\Omega}$.

SUMMARY

In an attempt to quantitatively examine the effect of variable rotor speed on the longitudinal static stability of an autorotating rotor, expressions have been developed for the changes in rotor forces under a condition of maintenance of constant zero torque. Force and moment derivatives were then calculated for a small autogyro rotor under two limiting conditions, i.e. for rotor speed assumed constant throughout velocity and attitude perturbations and for rotor speed varying in such a way that equilibrium torque is maintained throughout the perturbations. Comparison of the two conditions showed that allowing rotor r.p.m. to vary caused the velocity stability, M_V, to go from a strong stable condition at constant r.p.m. to a neutrally stable condition. The effect on angle of attack stability was to cause an unstable condition at constant r.p.m. to become stable.

Static stability derivatives were calculated for a small autogyro under the variable rotor speed conditions and steady state flight tests were conducted to attempt to verify these derivatives from trim curves. Although the flight tests tended to confirm the results, they were felt to be inconclusive in that they could only verify ratios of the derivatives. Using the constant coefficient of the characteristic or "frequency" equation as a measure of static stability the aircraft was determined to be statically stable. Further, the variation of rotor speed improved the static stability although it did reduce the velocity stability.

It was further concluded that the static stability of the aircraft was independent of horizontal c.g. position as long as the range of c.g. movement was confined to control limits.

AN INVESTIGATION OF THE LONGITUDINAL STATIC STABILITY OF AN AUTOGYRO

1. INTRODUCTION

It has been stated and is generally known that the articulated, lifting helicopter rotor in forward flight is statically stable with respect to velocity changes and is statically unstable with respect to change of angle of attack. This statement implies the classical rigid rotor with no artificial type of stabilization device and further assumes that the rotational speed of the rotor is constant.

Gessow and Myers (Ref. 1) state that the autorotating rotor has different stability characteristics than the powered rotor. The primary reason for this difference is the fact that the rotor speed of the autorotating rotor is not controlled by the engine, but is free to vary with change in forward speed or angle of attack. Hohenemser (Ref. 2) states that the effect of these variations in rotor speed is to make the autorotating rotor neutrally stable with changes in speed at constant angle of attack and positively stable with change in angle of attack at constant speed.

It is, therefore, the objective of this paper to derive expressions for the longitudinal static stability of the autorotating rotor in forward flight, to examine the effect of allowing the rotor

speed to vary, and to attempt to verify the results qualitatively, if not quantitatively, by simple equilibrium flight testing of a small, one-man autogyro. See Figure 1.

Throughout the analysis stability derivatives will be kept in a dimensional form to retain the physical concepts; and the physical quantities of the test aircraft, as listed in Appendix I, will be used.

II. ANALYSIS

In the stability analysis of any vehicle, it is first necessary to establish a system of coordinates to describe the motions of the vehicle. Since actual flight testing is involved in this analysis, it is felt that the "stability-axis" system where the origin of coordinates is placed at the c.g. of the aircraft and the positive X axis fixed in the aircraft and initially oriented into the relative wind is best suited. Figure 2 shows the axis system and various quantities relative to it.

How to accurately describe the motion of the vehicle depends upon the number of degrees of freedom it has and how strongly each degree affects the motions. As it is our purpose to examine the longitudinal static stability and to determine the effect of the rotor's rotational degree of freedom upon it, certain simplifying assumptions are necessary to avoid making the calculations so complex that an engineering analysis becomes impractical. It is first assumed that the longitudinal and lateral motions of the aircraft are loosely coupled, so that the longitudinal motions may be effectively described by the classic three degree of freedom equations, i.e. X Force, Z Force, and Pitching Moment. The rotor itself has six degrees of freedom, i.e. coning, lateral and longitudinal flapping and steady, longitudinal, and lateral twisting, plus the freedom of rotational speed. Under the assumption of a rigid rotor, which is usually valid for stability analysis, and writing the rotor statics in terms of fuselage variables, the rotor degrees of freedom may be reduced to the variation of rotor speed.

Further, since steady state flight test techniques are not completely suitable for the rate derivative, rate and acceleration terms will be omitted from the equations of motion.

Z Force Equation

Summing forces along the Z axis (see Figure 2) and neglecting any fuselage lift as small compared to the rotor forces gives

$$\Sigma F_Z = W\cos\gamma - T\cos\alpha + H\sin\alpha \tag{1}$$

For small angles, the cosine may be taken as equal to unity. Neglecting $H\sin\alpha$ as the product of small quantities, the Z force equation reduces to

$$\Sigma F_Z = W-T \tag{2}$$

Taking increments

$$\Sigma F_Z + \Delta F_Z = W-(T+\Delta T) \tag{3}$$

Subtracting equation (2) from (3)

$$\Sigma \Delta F_Z = -\Delta T \tag{4}$$

In terms of the rotor

$$\Delta T = \frac{T}{V}\Delta V + \frac{\partial T}{\partial \alpha_1}(\Delta\alpha_1 + \Delta\xi) + \frac{\partial T}{\partial a_1}\Delta a_1 + \frac{\partial T}{\partial \dot{a}_1}\Delta \dot{a}_1 + \frac{\partial T}{\partial \omega_1}\Delta\omega_1$$
$$+ \frac{\partial T}{\partial \dot{\omega}_1}\Delta\dot{\omega}_1 + \frac{\partial T}{\partial \Omega}\Delta\Omega + \frac{\partial T}{\partial \theta}\Delta\theta \tag{5}$$

If the approximation is made that the rotor is restrained to move in the plane of symmetry in determination of rotor thrust and that the

derivative $\frac{\partial T}{\partial a_1}$ is negligibly small as is suggested in Ref. , then for a fixed blade pitch

$$\Delta T = \frac{\partial T}{\partial V}\Delta V + \frac{\partial T}{\partial \alpha}(\Delta \alpha_1 + \Delta \delta) + \frac{\partial T}{\partial \Omega}\Delta\Omega \qquad (6)$$

Included in equation (6) is the term $\frac{\partial T}{\partial \Omega}\Delta\Omega$ implying the change of rotor speed as an independent variable. Examination of the torque equation for an autorotating rotor

$$b I_{rotor}\dot{\Omega} + Q_{aerodynamic} = 0 \qquad (7)$$

shows that for steady state conditions the aerodynamic torque must equal zero. If the assumption is made that the inertia of the rotor is negligible then the speed variation of the rotor is dependent on torque equilibrium. This assumption allows us to make rotor speed a dependent variable and eliminate the torque equation from the equations of motion. Further defining the rotor force derivatives in a special way such that $\left.\frac{\partial T}{\partial \alpha}\right|_{Q=0}$ means the rate of change of rotor thrust with angle of attack while forward velocity is held constant but rotor speed is allowed to vary in accordance with torque equilibrium, then equation (6) may be written

$$\Delta T = \left.\frac{\partial T}{\partial V}\right|_{Q=0}\Delta V + \left.\frac{\partial T}{\partial \alpha}\right|_{Q=0}(\Delta \alpha_1 + \Delta \delta) \qquad (8)$$

and the summation of force changes in the Z direction for equilibrium flight is

$$\Sigma\Delta F_Z = \left.\frac{\partial Z}{\partial V}\right|_{Q=0} \Delta V + \left.\frac{\partial Z}{\partial \alpha}\right|_{Q=0} (\Delta\alpha_1 + \Delta\delta) \qquad (9)$$

where

$$\left.\frac{\partial Z}{\partial V}\right|_{Q=0} = - \left.\frac{\partial T}{\partial V}\right|_{Q=0} \qquad (9a)$$

$$\left.\frac{\partial Z}{\partial \alpha}\right|_{Q=0} = - \left.\frac{\partial T}{\partial \alpha}\right|_{Q=0}$$

Pitching Moment Equation

Again referring to Fig. 2, the moments about the aircraft c.g. may be written as follows

$$\Sigma M_{cg} = \bar{x}(T\cos\delta - H\sin\delta) - \bar{z}(T\sin\delta + H\cos\delta) + M_e + M_{f_p} \qquad (10)$$

Since the rotor on the aircraft being investigated is a see-saw type the moment due to flapping hinge eccentricity, M_e, is zero. This moment can otherwise often be neglected if the flapping hinge offset is small. Further assuming small angles and neglecting $H\delta$ as the product of small quantities

$$\Sigma M_{cg} = \bar{x}T - \bar{z}\ (T\delta + H) + M_{f_p} \qquad (11)$$

Taking increments

$$\Sigma M_{cg} + \Delta M_{cg} = \bar{x}(T + \Delta T) - \bar{z}\ [(T+\Delta T)(\delta+\Delta\delta)+(H+\Delta H)] + M_{f_p} + \Delta M_{f_p} \qquad (12)$$

Subtracting equation (11) from (12)

$$\Sigma\Delta M_{cg} = \bar{x}\Delta T - \bar{z}\ (\Delta T\delta+\Delta\delta T + \Delta H) + \Delta M_{f_p} \qquad (13)$$

Substituting into equation (13)

$$\Delta T = \left.\frac{\partial T}{\partial V}\right|_{Q=0} \Delta V + \left.\frac{\partial T}{\partial \alpha}\right|_{Q=0} (\Delta\alpha_1 + \Delta\delta) \qquad (\quad)$$

$$\Delta H = \left.\frac{\partial H}{\partial V}\right|_{Q=0} \Delta V + \left.\frac{\partial H}{\partial \alpha}\right|_{Q=0} (\Delta K_1 + \Delta\delta) \qquad (15a)$$

$$\Delta M_{f_p} = \frac{\partial M_{f_p}}{\partial V}\Delta V + \frac{\partial M_{f_p}}{\partial \alpha_1}\Delta\alpha_1 \qquad (15b)$$

yields the following

$$\begin{aligned}\Sigma\Delta M_{cg} = {} & \left(\bar{x}\left.\frac{\partial T}{\partial V}\right|_{Q=0} - \bar{z}\delta\left.\frac{\partial T}{\partial V}\right|_{Q=0} - \bar{z}\left.\frac{\partial H}{\partial V}\right|_{Q=0} + \frac{\partial M_{f_p}}{\partial V}\right)\Delta V \\ & + \left(\bar{x}\left.\frac{\partial T}{\partial \alpha}\right|_{Q=0} - \bar{z}\delta\left.\frac{\partial T}{\partial \alpha}\right|_{Q=0} - \bar{z}\left.\frac{\partial H}{\partial \alpha}\right|_{Q=0} + \frac{\partial M_{f_p}}{\partial \alpha_1}\right)\Delta\alpha_1 \\ & + \left(\bar{x}\left.\frac{\partial T}{\partial \alpha}\right|_{Q=0} - \bar{z}\delta\left.\frac{\partial T}{\partial \alpha}\right|_{Q=0} - \bar{z}\left.\frac{\partial H}{\partial \alpha}\right|_{Q=0} - zT\right)\Delta\delta\end{aligned} \qquad (14)$$

Considering equation (14)

$$\Sigma\Delta M_{cg} = \left.\frac{\partial M}{\partial V}\right|_{Q=0}\Delta V + \left.\frac{\partial M}{\partial \alpha}\right|_{Q=0}\Delta\alpha_1 + \left.\frac{\partial M}{\partial \delta}\right|_{Q=0}\Delta\delta \qquad (15)$$

where

$$\left.\frac{\partial M}{\partial V}\right|_{Q=0} = \left(\left.\frac{\partial M}{\partial V}\right|_{Q=0}\right)_{\text{rotor}} + \frac{\partial M_{f_p}}{\partial V} \qquad (15a)$$

$$\left.\frac{\partial M}{\partial V}\right|_{Q=0}_{\text{rotor}} = \bar{x}\left.\frac{\partial T}{\partial V}\right|_{Q=0} - \bar{z}\delta\left.\frac{\partial T}{\partial V}\right|_{Q=0} - \bar{z}\left.\frac{\partial H}{\partial V}\right|_{Q=0} \qquad (15b)$$

$$\left.\frac{\partial M}{\partial \alpha}\right|_{Q=0} = \left(\left.\frac{\partial M}{\partial \alpha}\right|_{Q=0}\right)_{\text{rotor}} + \frac{\partial M_{f_p}}{\partial \alpha_1} \qquad (15c)$$

$$\left.\frac{\partial M}{\partial \alpha}\right|_{Q=0}_{\text{rotor}} = \bar{x}\left.\frac{\partial T}{\partial \alpha}\right|_{Q=0} - \bar{z}\delta\left.\frac{\partial T}{\partial \alpha}\right|_{Q=0} - \bar{z}\left.\frac{\partial H}{\partial \alpha}\right|_{Q=0} \qquad (15d)$$

$$\left.\frac{M}{\partial}\right|_{Q=0} = \left(\left.\frac{M}{\partial}\right|_{Q=0}\right)_{rotor} - \frac{\partial T}{\partial} \tag{16c}$$

Equations of Motion

The previously developed equations of motion for steady state flight conditions can now be written

$$\left.\frac{\partial Z}{\partial V}\right|_{Q=0} V + \left.\frac{\partial Z}{\partial \alpha}\right|_{Q=0} \Delta\alpha_1 + \left.\frac{\partial Z}{\partial \delta}\right|_{Q=0} \Delta\delta = 0 \tag{16a}$$

$$\left.\frac{\partial M}{\partial V}\right|_{Q=0} V + \left.\frac{\partial M}{\partial \alpha}\right|_{Q=0} \Delta\alpha_1 + \left.\frac{\partial M}{\partial \delta}\right|_{Q=0} \Delta\delta = 0 \tag{16b}$$

And it is possible to make a qualitative check on the derivatives by comparing the slope of the trim curves taken from steady state flight test to the predicted slopes, since they may now be predicted from equations 16.

$$\frac{\Delta\delta}{\Delta V} = \frac{Z_\alpha M_V - Z_V M_\alpha}{A_\alpha (M_\delta - M_\dot{\alpha})} \tag{17a}$$

$$\frac{\Delta\alpha_1}{\Delta V} = \frac{Z_V M_\delta - Z_\delta M_V}{Z_\alpha (M_\alpha - M_\delta)} \tag{17b}$$

A check on the rotor thrust derivatives may also be made by noting from equation (16a) (since $\Delta\alpha = \Delta\alpha_1 + \Delta\delta$)

$$\frac{\Delta\delta}{\Delta V} = -\frac{Z_V}{Z_\alpha} \tag{17c}$$

Further, the effect of variation of rotor speed on each particular derivative is available by computing each one separately under the

assumption of constant rotor speed, letting the rotor speed derivatives $\left.\frac{\partial \Omega}{\partial V}\right|_{\alpha} = \left.\frac{\partial \Omega}{\partial \alpha}\right|_{V} = 0$, and drop those terms.

Evaluation of the Derivatives

From the definition of the rotor thrust coefficient

$$T = \rho \pi R^2 (\Omega R)^2 C_T \tag{18}$$

where Ω is the trim value. Letting $K_1 = \rho \pi R^2 (\Omega R)^2$, then

$$\frac{\partial T}{\partial V} = K_1 \frac{\partial C_T}{\partial V} \tag{19a}$$

$$\frac{\partial T}{\partial \alpha} = K_1 \frac{\partial C_T}{\partial \alpha} \tag{19b}$$

$$\frac{\partial T}{\partial \Omega} = K_1 \left[\frac{\partial C_T}{\partial \Omega} + \frac{2 C_T}{\Omega} \right] \tag{19c}$$

Including Ω as an independent variable requires the addition of the torque equation to the equations of motion. As we have already seen, however, neglecting the inertia of the rotor allows us to make Ω a dependent variable, and the rotor thrust derivatives could be expressed as

$$\left.\frac{\partial T}{\partial V}\right|_{Q=0} = K_1 \left[\frac{\partial C_T}{\partial V} + \left.\frac{\partial \Omega}{\partial V}\right|_{Q=0} \left(\frac{\partial C_T}{\partial \Omega} + \frac{2 C_T}{\Omega} \right) \right] \tag{20a}$$

$$\left.\frac{\partial T}{\partial \alpha}\right|_{Q=0} = K_1 \left[\frac{\partial C_T}{\partial \alpha} + \left.\frac{\partial \Omega}{\partial \alpha}\right|_{Q=0} \left(\frac{\partial C_T}{\partial \Omega} + \frac{2 C_T}{\Omega} \right) \right] \tag{20b}$$

Evaluation of the thrust coefficient derivatives may be made from blade element theory, where the thrust coefficient is given by

$$\frac{2 C_T}{a \sigma} = \theta \left(\frac{B^3}{3} + B \mu^2 \right) + \lambda \left(\frac{B^2}{2} + \frac{\mu^2}{4} \right) \tag{21}$$

For a constant blade pitch angle the thrust coefficient is a function of the variables μ and λ

$$C_T = C_T(\mu,\lambda)$$

If the usual assumption for the average induced velocity of a lightly loaded rotor in forward flight is taken from momentum theory as

$$v = \frac{T}{2\rho\pi R^2 V'} \tag{22}$$

where V' is the resultant velocity at the rotor disk, then the inflow ratio, λ, may be expressed as

$$\lambda = \mu\tan\alpha - \frac{C_T}{2\sqrt{\mu^2+\lambda^2}} \tag{23}$$

Since by definition the tip speed ratio, μ, is given by

$$\mu = \frac{V\cos\alpha}{\Omega R} \tag{24}$$

It then follows that the thrust coefficient could be expressed as a function of the variables V, α, and Ω.

$$C_T = C_T(V,\alpha,\Omega) \tag{25}$$

The thrust coefficient derivatives may then be evaluated following the chain rule for partial differentiation

$$\frac{\partial C_T}{\partial V} = \frac{\partial C_T}{\partial \mu}\frac{\partial \mu}{\partial V} + \frac{\partial C_T}{\partial \lambda}\frac{\partial \lambda}{\partial V} \tag{26a}$$

$$\frac{\partial C_T}{\partial V_m} = \frac{\partial C_T}{\partial \mu}\frac{\partial \mu}{\partial V} + \frac{\partial C_T}{\partial \lambda}\frac{\partial \lambda}{\partial V}$$

$$\frac{\partial C_T}{\partial \Omega} = \frac{\partial C_T}{\partial \mu}\frac{\partial \mu}{\partial \Omega} + \frac{\partial C_T}{\partial \lambda}\frac{\partial \lambda}{\partial \Omega}$$

Note that due to the relation between inflow ratio and thrust coefficient through the momentum theory, the inflow ratio derivatives are a little complicated and have a character somewhat more like total derivatives

$$\frac{\partial \lambda}{\partial V} = \frac{\mu}{V}\left[\frac{\tan\alpha - \dfrac{\dfrac{\partial C_T}{\partial \mu}}{2\sqrt{\mu^2+\lambda^2}} + \dfrac{\mu C_T}{2(\mu^2+\lambda^2)^{3/2}}}{1 + \dfrac{\dfrac{\partial C_T}{\partial \mu}}{2\sqrt{\mu^2+\lambda^2}} - \dfrac{\mu C_T}{2(\mu^2+\lambda^2)^{3/2}}}\right]$$

$$\frac{\partial \lambda}{\partial \alpha} = \mu\tan\alpha\left[\frac{\cot\alpha + \dfrac{\dfrac{\partial C_T}{\partial \mu}}{2\sqrt{\mu^2+\lambda^2}} - \dfrac{\mu C_T}{2(\mu^2+\lambda^2)^{3/2}}}{1 + \dfrac{\dfrac{\partial C_T}{\partial \lambda}}{2\sqrt{\mu^2+\lambda^2}} - \dfrac{C_T}{2(\mu^2+\lambda^2)^{3/2}}}\right]$$

$$\frac{\partial \lambda}{\partial \Omega} = -\frac{\mu}{\Omega}\left[\frac{\tan\alpha - \dfrac{\dfrac{\partial C_T}{\partial \mu}}{2\sqrt{\mu^2+\lambda^2}} + \dfrac{\mu C_T}{2(\mu^2+\lambda^2)^{3/2}}}{1 + \dfrac{\dfrac{\partial C_T}{\partial \lambda}}{2\sqrt{\mu^2+\lambda^2}} - \dfrac{\mu C_T}{2(\mu^2+\lambda^2)^{3/2}}}\right]$$

Some simplification is possible in the inflow ratio derivatives by neglecting λ^2 compared to μ^2 at tip speed ratios above about 0.10 and approximating the inflow ratio as

$$\lambda = \mu\alpha - \frac{C_T}{2\mu}$$

Since much of the range of flight being investigated was below $\mu = 0.10$, this simplification was not used in the included calculations.

Evaluation of the rotor speed derivatives must evolve from the torque relation, since it is the change of rotor speed in accordance with torque equilibrium that is desired. From Bailey's aerodynamic torque relations (Ref. 4) the aerodynamic torque may be expressed as a function of the tip speed ratio and inflow ratio. For a fixed blade pitch angle then:

$$C_Q = C_Q(\mu,\lambda) \quad .$$

See Appendix II for complete torque relations. Since the only torque acting on the autorotating rotor at equilibrium is aerodynamic torque it follows that

$$C_Q = 0$$

and the inflow ratio may be determined in terms of the tip speed ratio. This has been computed for the rotor being investigated and is plotted on Figure 3.

From the definitions of the tip speed ratio and inflow ratio the aerodynamic torque coefficient may be expressed as a function of the variables V, α, and Ω.

It follows that

$$\Delta C_Q = \frac{\partial C_Q}{\partial V}\Delta V + \frac{\partial C_Q}{\partial \alpha}\Delta\alpha + \frac{\partial C_Q}{\partial \Omega}\Delta\Omega$$

Having neglected the inertia of the rotor as having a negligible effect on rotor speed perturbations, the equilibrium torque must be maintained. Then

$$\Delta C_Q = 0$$

so that

$$\left.\frac{\partial \Omega}{\partial V}\right|_{\alpha} = -\frac{\frac{\partial C_Q}{\partial V}}{\frac{\partial C_Q}{\partial \Omega}}$$

$$\left.\frac{\partial \Omega}{\partial \alpha}\right|_{V} = -\frac{\frac{\partial C_Q}{\partial \alpha}}{\frac{\partial C_Q}{\partial \Omega}}$$

These particular derivatives may be evaluated by direct differentiation; they have been so performed for the rotor being investigated, and are plotted on Figures 4 and 5 as functions of the tip speed ratio, μ.

Substituting equations (27) and (25) back into (20) determines the rotor thrust derivatives under the varying rotor speed conditions. These derivatives, along with thrust derivatives computed on the assumption of constant rotor speed, have been computed for the rotor being investigated and are plotted on Figures 6 and 7.

Since the trim values of the inflow ratio λ can be calculated from the aerodynamic torque relation in terms of the tip speed ratio μ, as is shown in Appendix II and plotted on Figure 3, the trim thrust

coefficient, C_T, is determined from blade element theory, equation (11). This has been done and the trim thrust coefficient is plotted as a function of the tip speed ratio on Figure 5. For a given gross weight then, the trim rotor speed may be obtained from equation (11). The trim value of the angle of attack of the plane of no feathering is determined from equation (23), and trim forward speed is determined from the definition of the tip speed ratio, equation (24).

Evaluation of the moment derivatives, equations (11), requires a knowledge of the H force derivatives, trim control angle θ, and fuselage and power contributions to stability, M_{f_p}, as well as the rotor thrust derivative. The rotor H force coefficient as given by Gessaw and Myers (ref. 1) for the H force in the plane of no feathering is

$$\frac{2C_H}{a\sigma} = \frac{\mu\bar{\delta}}{2a} + \frac{\theta_{.75}}{3} - \frac{\mu\theta}{2} + \frac{3\lambda_1}{4} + \frac{\mu a_1}{4} - \frac{a_{0_1}}{3} + \frac{\mu a_0^2}{4} \tag{28}$$

Since the flapping angles relative to the plane of no feathering can be expressed as functions of the tip speed ratio and inflow ratio (the coning angle for the see-saw rotor, a_0, is built in and constant) they may be substituted into the H force coefficient equation and it may be completely expressed as a function of μ and λ.

$$a_1 = \frac{1}{\frac{B^4}{2} - \frac{\mu^2 B^2}{4}} \left[\mu\lambda\left(B^2 - \frac{\mu^2}{4}\right) + \frac{4}{3}\theta\mu B^3 \right] \tag{29a}$$

$$b_1 = \frac{\frac{4}{3}\mu B a_0}{B^2 + \frac{\mu^2}{4}} \tag{29b}$$

$$C_H = C_H(\mu, \lambda)$$

Having obtained α as a function of μ from torque equilibrium, the trim H force coefficient is therefore determined, and has been plotted in Figure 8. Further, knowing the trim rotor speed determines the H force itself from the definition of the H force coefficient

$$C_H = \frac{H}{\rho \pi R^2 (\Omega R)^2} \tag{30}$$

The H force has been calculated for the rotor under investigation and is plotted on Figure 9 as a function of tip speed ratio μ.

From the definition of the H force coefficient, equation (30), the H force derivatives may be obtained in a similar manner to that used for the thrust force coefficients.

$$\frac{\partial H}{\partial V} = K_1 \frac{\partial C_H}{\partial V} \tag{31a}$$

$$\frac{\partial H}{\partial \alpha} = K_1 \frac{\partial C_H}{\partial \alpha} \tag{31b}$$

$$\frac{\partial H}{\partial \Omega} = K_1 \left[\frac{\partial C_H}{\partial \Omega} + \frac{2C_H}{\Omega} \right] \tag{31c}$$

Evaluation of the H force derivatives under conditions of variable rotor speed also follows similarly:

$$\left.\frac{\partial H}{\partial V}\right|_{Q=0} = K_1 \left[\frac{\partial C_H}{\partial V} + \left.\frac{\partial \Omega}{\partial V}\right|_{\alpha} \left(\frac{\partial C_H}{\partial \Omega} + \frac{2C_H}{\Omega} \right) \right] \tag{32a}$$

$$\left.\frac{\partial H}{\partial \alpha}\right|_{Q=0} = K_1 \left[\frac{\partial C_H}{\partial \alpha} + \left.\frac{\partial \Omega}{\partial \alpha}\right|_{V} \left(\frac{\partial C_H}{\partial \Omega} + \frac{2C_H}{\Omega} \right) \right] \tag{32b}$$

Since the H force coefficient can be expressed completely in terms of the tip speed ratio μ and inflow ratio λ by substitution of the flapping angle relations, equations (29), into equation (28), it follows that:

$$C_H = C_H(V,\alpha,C) \tag{33}$$

The H force coefficient derivatives may be evaluated by differentiation in a manner similar to that used to obtain the thrust force coefficient derivatives.

The rotor H force derivatives have been calculated for both constant r.p.m. and variable r.p.m. as indicated above, and are presented on Figures 10 and 11.

To find the trim control angle δ it is necessary to solve the moment equation, equation (11), for trim conditions

$$\Sigma M_{cg} = \bar{x}T - \bar{z}(T\delta + H) + M_{f_p} = 0 \tag{34}$$

which necessitates an estimation of the moment about the c.g. due to fuselage and power effects, M_{f_p}. To a first approximation it is felt that the fuselage itself will have little aerodynamic moment, if any. It does, however, have a small, flat plate horizontal tail surface which may offer an appreciable moment at higher angles of attack. The tail contribution to trim moments would be

$$M_t = x_t S_t a_t \alpha_t q \tag{35}$$

Power effects are difficult to estimate accurately. A small amount is contributed due to direct propeller thrust as the thrust axis is offset a small distance from the c.g.

$$M_{T_p} = z_p T_p \tag{36}$$

A propeller normal force will exist when the thrust axis (parallel to the fuselage reference line) operates at an angle of attack. Following the method of Ribner (Ref. 5) a propeller normal force based on propeller thrust coefficient and propeller geometry has been estimated. The moment due to propeller normal force can then be expressed as

$$M_{N_p} = x_p \frac{\partial N_p}{\partial \alpha} \alpha_p \tag{37}$$

Since the total pitching moment due to fuselage and power effects is now available,

$$M_{f_p} = M_f + M_{T_p} + M_{N_p} \tag{38}$$

and noting that

$$\alpha_t = \alpha_f = \alpha_p = \alpha - i_R \tag{39}$$

the trim control angle δ may now be obtained by substituting equation (38) into (34) and rearranging.

$$\delta = \frac{\bar{x}T - \bar{z}H + x_f S_f a_f q(\alpha - i_R) + z_p T_p + x_p \frac{\partial N_p}{\partial \alpha}(\alpha - i_R)}{\bar{z}T + x_T S_f a_f q + x_p \frac{\partial N_p}{\partial \alpha}} \tag{40}$$

Note that the power moments require an estimation of the thrusting propeller force, which may be obtained by solving the horizontal trim force equation:

$$\Sigma F_x = T_p \cos\alpha_p - T_\alpha \sin\alpha - H\cos\alpha - D_f - W\sin\gamma = 0 \qquad (41)$$

assuming small angles

$$T_p = T_\alpha + H + D_f + W\gamma \qquad (42)$$

Estimation of the contribution of fuselage and power effects to the static stability of the aircraft, M_{f_p}, will probably introduce as great an error as any other approximation. As was indicated in the analysis for the trim control angle, δ, the fuselage is assumed to have a negligible moment of itself. No known theory is available to predict a moment for this frame-like structure and without wind tunnel data, it can only be assumed small. Tail contribution to stability can be estimated from equation (3):

$$\frac{\partial M_t}{\partial V} = x_t \delta_{t_p} \alpha_t \partial V \qquad (43a)$$

$$\frac{\partial M_t}{\partial \alpha} = x_t \delta_{t_a} q \qquad (43b)$$

Since the moment arm of the thrust axis is quite small and no simple theory exists for estimation of the engine thrust changes with velocity for constant pitch propellers, the direct propeller thrust contribution is also neglected. The propeller normal force contribution to stability is taken from equation (37):

$$\frac{\partial M_{N_p}}{\partial \alpha} = x_p \frac{\partial N_p}{\partial \alpha}$$

The tail and propeller normal force contributions to stability have been calculated as indicated above and are presented on Figure 12.

With estimates of the rotor force derivatives, trim control angle, and fuselage and power contributions available, equations (15) may now be solved for the moment derivatives. The derivatives have been obtained for the rotor alone for both constant rotor speed and variable rotor speed conditions in accordance with torque equilibrium and are presented on Figures 13 and 14. Further, the aircraft derivatives have been calculated by including the fuselage and power effects and are presented on Figures 15, 16, and 17.

III. EQUIPMENT AND PROCEDURE

Aircraft

The aircraft used to obtain trim data for this analysis was a small, one-man autogyro known as a Bensen B-8M "Gyrocopter." See Figure 1. The aircraft, built and flown by the author, is powered by a 72 HP McCulloch air cooled, four cylinder, two cycle engine driving a fixed pitch Banks and Maxwell pusher propeller. The rotor is a see-saw or "teetering" rotor with a diameter of 20 feet and a constant blade chord of 6-3/4 inches. The blades are untwisted, have a fixed blade pitch angle of 1½ degrees, and a built-in coning angle of 4 degrees. Control is affected through an overhead control stick connected directly to the rotor shaft by two bearings. The rotor shaft is free to rotate 10 degrees laterally and longitudinally about the main thrust bearing in the control head (rotor reference axis). A conventional vertical fin and rudder is immersed in the propeller slipstream at the tail to control sideslip. A small, fixed, flat plate horizontal tail surface is mounted directly under the engine and functions both as stabilizing surface and propeller shield when taxiing. The aircraft weighs 225 pounds empty and 400 pounds at normal gross weight.

Instrumentation

Airspeed and Altitude

A standard helicopter airspeed indicator and sensitive altimeter were used to determine airspeed and altitude. The instruments were

driven by a swivelling static pressure probe and a shielded total head pick-up, both mounted on a small boom on the forward portion of the aircraft. The airspeed system was calibrated by the standard speed course method and the calibration curve is presented on Figure 18.

Rotor Speed

Rotor speed was obtained by driving a Servo-Tek Products linear tachometer-generator with a short, flexible shaft directly from the rotor shaft and was displayed on a shunted micro-ammeter mounted on the instrument panel. The system was calibrated by driving the tachometer-generator with a variable speed drill motor and measuring r.p.m. with a stroboscope. The micro-ammeter was then biased so that it read rotor r.p.m. directly. The accuracy of the system was within the ability of the pilot to read the ammeter, which is felt to be $\pm$ 2 r.p.m. Rotor r.p.m. was used only as a check on the predicted thrust coefficients.

Control Angle

Control angle, corresponding to stick position, was measured by mounting a 750 ohm potentiometer on the mast just below the rotor control head. A waxed nylon line wrapped several turns around a pulley on the potentiometer shaft had one end connected to the aircraft frame through a tension spring and the other end connected to a short, rigid arm mounted on the movable rotor head. The tension provided by the spring allowed the wiper of the potentiometer to follow the longitudinal movement of the rotor shaft. The potentiometer was driven by two 1.34 volt mercury batteries and the output was displayed on a micro-ammeter mounted on the instrument panel. The system was calibrated by measuring control

angle with a propeller protractor and loading the ammeter with a 50,000 ohm potentiometer in series with it. The ammeter was so calibrated to read control angle directly in degrees, and the accuracy of the system was within the pilot's ability to read the ammeter, which is felt to be approximately ± 0.1 degree.

Fuselage Angle of Attack

Angle of attack of the fuselage reference line (see Figure 2) was measured by a small, balanced balsa wood vane mounted on the forward extremity of the aircraft. The vane was mounted on a horizontal shaft rotating in ball bearings and a pointer connected to the shaft read fuselage angle of attack on a scale on the vane frame. The system was call rated with a propeller protractor, and its accuracy is felt to be within ± 0.5 degrees.

Gross Weight and Center of Gravity Determination

The gross weight and center of gravity (c.g.) of the aircraft was obtained by three different methods as a cross check. First, they were obtained by computing the weight and balance of the various components. Secondly, the aircraft was weighed in various configurations with the fuselage reference line horizontal by three platform scales placed under the landing gear. This method gave gross weight and horizontal c.g. position only. Thirdly, the aircraft was hung from an overhead beam by dynamometer and cable attached to the rotor shaft. For various configurations the angle of inclination of the fuselage reference line and weight were determined. Knowing the inclination of the rotor head, a check could be obtained on both vertical

and horizontal c.g. position. The c.g. location thus obtained is felt to be accurate to within ± 0.25 inch in the horizontal direction and ± 0.50 inch in the vertical direction. The c.g. position (for the gross weight tested) relative to the rotor head is listed in Appendix I. It may be well to note that since the aircraft is relatively light, c.g. position can be affected by how the pilot sits in the seat. During flight testing every effort was made to maintain the c.g. position as determined above and gross weight is felt to be accurate to within ± 3 pounds.

Rotor Blade Section Characteristics

To accurately determine the section aerodynamic properties of the rotor blade a 12 inch section of the blade was tested in the Jones Forrestal Research Center two-dimensional wind tunnel. The results of the wind tunnel test are plotted on Figure 19. The section drag coefficient was corrected for Reynolds number effects to the average operating conditions at the 0.75R and expressed as a quadratic in section angle of attack. Section lift curve slope, drag coefficient, and blade pitch angle thus obtained are tabulated in Appendix I.

Procedure

The flight testing procedure followed was simply to establish steady-state level flight conditions at five knot intervals from 30 to 60 knots indicated forward speed, and record indicated speed, rotor rpm., control angle and fuselage angle of attack. Since all testing was done at altitudes of from 200 to 300 feet MSL, no temperature was measured in flight and density corrections were applied using corrected surface

temperature. The control angle versus velocity curve thus obtained is plotted on Figure 20, the rotor reference angle of attack versus velocity on Figure 21, and angle of attack of the no feathering plane versus velocity on Figure 22. The experimental thrust coefficient versus tip speed ratio obtained is plotted on Figure 8 for comparison with theoretical. Each point plotted represents an average of at least two readings.

IV. RESULTS AND DISCUSSION

The rotor force and moment derivatives have been calculated under assumed conditions of constant rotor speed and variable rotor speed in accordance with torque equilibrium, and are presented in Figures 6, 7, 10, 11, 13 and 14. The conditions of constant rotor speed and variable rotor speed in accordance with torque equilibrium are felt to be limiting conditions for autorotative rotor operation. The assumption of constant rotor speed could be interpreted to mean that the inertia of the rotor is very large (although it is usually justified by assuming that rotor speed changes are negligibly small); variable rotor speed was obtained through the assumption of negligible inertia. Obviously the real rotor has some inertia and its operation will lie somewhere between the two cases. For slow perturbations the rotor should tend to act more like the negligible inertia case; for rapid changes inertia will tend to maintain a constant rotor speed. The question naturally arises then as to how rapidly the rotor accelerates. Nikolsky indicates in work with a helicopter rotor of similar solidity in autorotation (Ref. 6) that the rotor reaches its peak acceleration in about $2\frac{1}{2}$ seconds. Using this figure only as an order of magnitude, it may be concluded that for long period dynamics the assumption of negligible inertia for the autorotating rotor is valid.

In the longitudinal plane static stability is usually defined as the restoring moment in relation to a change in forward linear velocity at constant angle of attack and in relation to a change in

angle of attack at constant velocity. A comparison of the velocity stability, M_V, (Figure 13) shows that the inertialess rotor is approximately neutrally stable while the constant speed rotor is quite stable. A comparison of the angle of attack stability, M_α (Figure 14), shows that the autorotating rotor becomes strongly stable due to rotor speed changes while the constant speed rotor is unstable. The static stability derivatives of the autorotating rotor of low inertia then behave more like a fixed wing than a helicopter rotor.

To qualitatively explain how the rotor speed variation affects the static stability consider a rotor in trim forward flight. An increase in forward velocity with constant angle of attack will cause a small increase in the rotor resultant force. Further, the increase in velocity will increase the longitudinal flapping angle causing a nose up or positive moment from trim if the rotor speed is constant. The rotational speed of the autorotating rotor increases with velocity; however, which causes the longitudinal flapping angle to decrease, resulting in a nose down or negative moment. When the rotor speed variation with forward speed occurs so that the equilibrium torque is maintained the net result is no variation in longitudinal flapping angle, and no moment is produced except due to the small increase in rotor resultant force. The autorotating rotor is therefore approximately neutrally stable with respect to speed. This fact could have been deduced by examining the aerodynamic torque relation. Since the torque can be expressed as a fucntion of μ and λ, it could further be expressed as a function of μ and α by appropriate substitution from momentum and blade element theory for λ and C_T. Since by assumption the equilibrium torque is

maintained, it then follows that the tip speed ratio is constant for perturbations at constant angle of attack. And since the longitudinal flapping angle can also be completely expressed as a function of μ and α by the same substitutions, it too must remain constant for perturbations at constant angle of attack. The method for quantitatively predicting the velocity stability of the autogyro developed in the analysis section did not yield identically neutral velocity stability. Since all the moments acting are aerodynamic (power effects have been neglected in velocity perturbations) then all the changes in moment at constant angle of attack are functions of velocity and the net result should have been identically neutral velocity stability. It is felt that the assumption of negligible fuselage moment and an overestimation of the tail contribution accounted for this apparent error.

To see the effect of variation of rotor speed on angle of attack stability consider again the rotor in trim forward flight. Increasing angle of attack and maintaining constant forward velocity will cause an increase in the rotor resultant force. The longitudinal flapping angle will also increase (for constant r.p.m.) tending to produce a further nose up or unstable moment. However, the increase in angle of attack will cause the autorotating rotor to increase rotor speed, resulting in a decrease in the longitudinal flapping angle and a further increase in resultant force. The net result for the autorotating rotor is to produce a nose down or stable moment due to the strong tendency for rotor speed to increase with angle of attack.

If the coefficient of the constant term of the characteristic or "frequency" equation is used as a measure of static stability (a necessary but not sufficient condition for dynamic stability):

$$E = W\cos\gamma(Z_V M_\alpha - Z_\alpha M_V) > 0 \text{ for static stability}$$

It is observed that the aircraft is statically stable for the assumed conditions of both constant and variable rotor speed. As shown on Figure 23 the static stability of the aircraft is improved by variable rotor speed due to the improvement in rotor angle of attack stability.

It can be shown that the static stability of the aircraft is independent of horizontal c.g. position provided that the c.g. travel is limited to the range where adequate control is available. Substituting equations (15a) and (15c) into the static stability, or E, term gives

$$E = W\cos\gamma \left[\bar{z}(Z_H M_V - Z_V H_\alpha) + Z_V \frac{\partial M_{f_p}}{\partial \alpha} - Z_\alpha \frac{\partial M_{f_p}}{\partial V} \right]$$

and is independent of $\bar{x}$. This could be physically reasoned by noting that the trim control angle δ is a strong function of the horizontal c.g. position through the pitching moment equilibrium equation, equation (40), and hence varying horizontal c.g. position will vary the trim control angle, but the static stability will not change. Varying the horizontal c.g. position will, of course, affect the stability contributions of fuselage and power by varying their moment arms but this is a secondary effect. Static stability can be improved by moving the c.g. vertically but is physically impractical for any significant improvement.

Trim curves of control angle, attitude angle, and angle of attack of the no-feathering plane respectively versus forward velocity taken from flight testing are presented on Figures 20, 21 and 22. A comparison of their measured and predicted slopes at various forward velocities is presented in Table I below.

Table I

V ft per sec		60	70	80	90	100
$\Delta\zeta$ / ΔV	Predicted	-0.000077	-0.000044	-0.000040	-0.000048	-0.000045
	Flight test	-0.000766	-0.000684	-0.000617	-0.000434	-0.000435
$\Delta\alpha$ / ΔV	Predicted	-0.00781	-0.00501	-0.00344	-0.00248	-0.00179
	Flight test	-0.00833	-0.00567	-0.0035	-0.00234	-0.00142
$\Delta\alpha$ / ΔV	Predicted	-0.00849	-0.00565	-0.00408	-0.00312	-0.00244
	Flight test	-0.0085	-0.00645	-0.00425	-0.00267	-0.00133

Considering the rather unsophisticated type of instrumentation used in flight testing and approximations necessary in the analysis, the correlation between predicted and measured data appears good. It is much better at lower forward velocities than high, due probably to a weaker influence of the unknown and neglected fuselage moments.

The perturbation equations of motion give us a relation between flight variables, such as V, α, and δ, and the stability derivatives which describe how the forces and moments act on the aircraft and which we wish to determine. Since each independent relation necessarily contains many of the flight variables it is seldom possible to obtain an explicit relation for any one unknown stability derivative in terms of the flight variables. It is possible in wind tunnel testing to hold all flight variables but one constant and measure the resultant change in forces or moments that act. Flight testing methods cannot hold all flight variables but one constant and measure the resulting changes because the aircraft cannot physically satisfy the equations of motion under these conditions. As a result steady state flight test methods usually attempt to hold as many flight variables as possible constant and verify

the stability derivatives through ratios of these variables. This has been done in this analysis by writing the perturbation equations in as simple a form as possible and still retaining the significant derivatives. The result is the two control-fixed steady-state perturbation equations (16a) and (16b)

$$Z_V \Delta V + Z_\alpha \Delta\alpha_1 + Z_\delta \Delta\delta = 0$$

$$M_V \Delta V + M_\alpha \Delta\alpha_1 + M_\delta \Delta\delta = 0$$

All the major stability derivatives (with the exception of pitch damping, a rate derivative) are contained in these two relations. By eliminating any one of the flight variables between the two equations a relation is obtained for the stability derivatives in terms of ratios of the two remaining flight variables. The ratios predicted in Table I were obtained from the above relations as

$$\frac{\Delta\delta}{\Delta V} = \frac{Z_\alpha M_V - Z_V M_\alpha}{Z_\alpha (M_\alpha - M_\delta)}$$

or

$$\frac{\Delta\alpha_1}{\Delta V} = \frac{Z_V M_\delta - Z_\alpha M_V}{Z_\alpha (M_\alpha - M_\delta)}$$

A further check on the Z force derivatives is obtained from the Z force equation, noting that $\Delta\alpha = \Delta\alpha_1 + \Delta\delta$

$$\frac{\Delta\alpha}{\Delta V} = -\frac{Z_V}{Z_\alpha} \quad .$$

If we had known one of the Z force derivatives from some independent source, such as a wind tunnel, then the other could be explicitly verified. Although steady-state flight test techniques have this disadvantage, their advantages of dissociation with phase lag problems and use of simplified instrumentation still make them attractive in many cases. Often, by selecting proper test techniques, it is possible to cross plot data to evaluate derivatives not otherwise obtainable, as is often done in fixed wing aircraft for the pitching moment-angle of attack stability derivative.

The flight test plot of control angle-velocity curve (Figure 20) shows a gradual decrease in the negative slope with forward velocity. The predicted slope of this curve is essentially constant. It is felt that the influence of the fuselage moments causes this decrease in slope at higher velocities, and neglecting these moments in the analysis resulted in the inability to predict the change. The concept of "stick-fixed" stability as used in fixed wing airplanes implies a definite relation between stick position and forward speed; that is, the stick position corresponding to a higher forward speed must be farther forward to be regarded as stable. Although the corollary is not necessarily warranted for rotary-winged aircraft, the autogyro tested is stable by this criteria. The fact that the slope decreases rather than increases with velocity could indicate a possible instability at some high forward speed. Hufton et.al., in an investigation of a British direct-control autogyro (Ref. 8) reported such a high speed instability, but determined the cause as blade twist.

The altitude angle-velocity and angle of attack of the no-feathering plane-velocity curves also show better correlation at the lower forward speeds, but an estimation of the accuracy of verifying the stability derivatives is difficult. In all cases below 90 f.p.s. the predicted slopes were within 12% of the flight test curves, which themselves undoubtedly contain some measurement error. The ratio of Z_V to Z_α verified by the slope of the angle of attack-velocity curve would easily point up any significant error in either one of the derivatives, but if the error existed in both derivatives by a constant factor, then the error could go undetected. Significant discrepancies in the predictions of the control angle-velocity or altitude angle-velocity ratios would be more difficult to analyze. Assuming the Z_V/Z_α ratio was verified, each ratio still contains the three moment derivatives. Due to the relative magnitudes of these three derivatives (M_V is very small compared to M_α and M_δ) a large error or even a change in sign could exist in M_V and would be difficult to verify. In fact, assuming neutral velocity stability for the aircraft as previously discussed improves the correlation. Since the M_δ derivative is essentially the rotor M_α plus a constant term, the control angle and altitude angle curves essentially verify the pitching moment-angle of attack stability derivative, which, as pointed out, becomes increasingly difficult to predict at higher velocities.

In summary it is felt that the trim curves tend to verify the vertical force derivatives and angle of attack stability, and can point out possible unstable areas not predicted by analysis. Neutral velocity stability for the aircraft is felt to be a reasonable approximation.

V. CONCLUSIONS

As a result of this analysis the following conclusions are felt to be valid:

1. The method developed in this analysis for predicting static stability derivatives is valid, but is limited by fuselage effects.
2. The autorotating rotor is approximately neutrally stable with respect to velocity changes.
3. The autorotating rotor is statically stable with respect to altitude change.
4. The static stability of the direct control type rotor is independent of horizontal c.g. position as long as it is within control limits.
5. The direct control type autogyro considered is statically stable, due in large part to the ability of the rotor to change speed during perturbations.
6. Trim curves tend to verify the method developed for computing static stability derivatives, but by themselves are not conclusive.

VI. REFERENCE

1. Gessow, A. and Myers, G. C., Aerodynamics of the Helicopter, The Macmillan Company, New York, 1967.

2. Hohenemser, K., "A Type of Lifting Rotor with Inherent Stability." J. A. S., Vol. 17, No. 9, September, 1950.

3. Deazley, W. R. and Schultz, E. R., The Determination of Helicopter Longitudinal Stability Derivatives from Flight Test Data, Part I. WADC TR 55-436, February, 1958.

4. Bailey, F. J., Jr., A Simplified Theoretical Method of Determining the Characteristics of a Lifting Rotor in Forward Flight. NACA TR-716, 1941.

5. Ritner, H. L., Notes on the Propeller and Slip-stream in Relation to Stability. NACA WRL25, 1944.

6. Nikolsky, A. A., The Stability and Control of Single Rotor Helicopters in Autorotative Forward Flight. Princeton University Aeronautical Engineering Dept. Report No. 215, October, 1952.

7. Shapiro, J., Principles of Helicopter Engineering, McGraw-Hill Inc., New York, 1955.

8. Hufton, P. A.; Nutt, A. E. T.; Bigg, F. J. and Beaver, J. A., General Investigation into the Characteristics of the C-30 Autogyro, British R&M 1859.

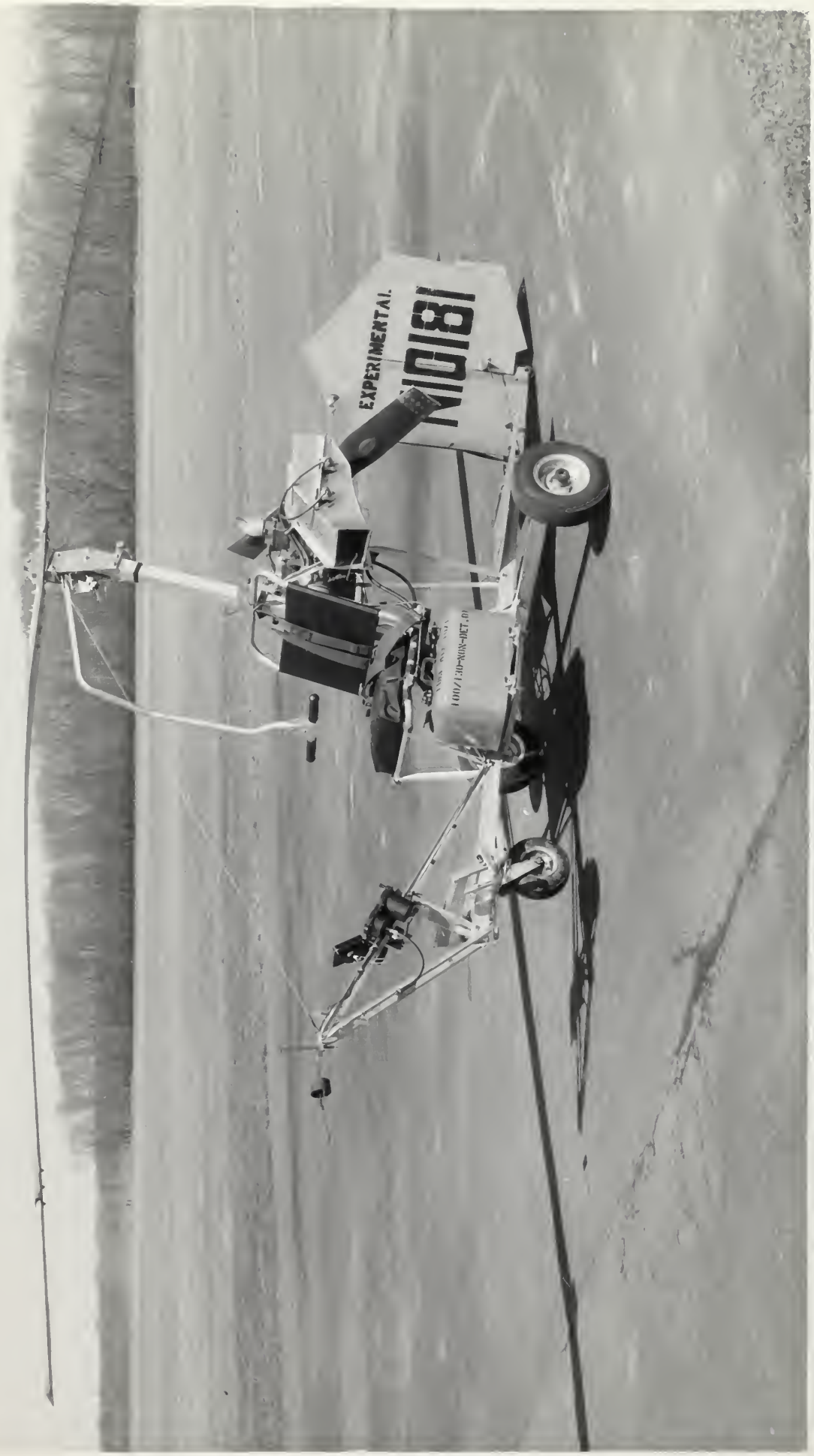

Figure #1

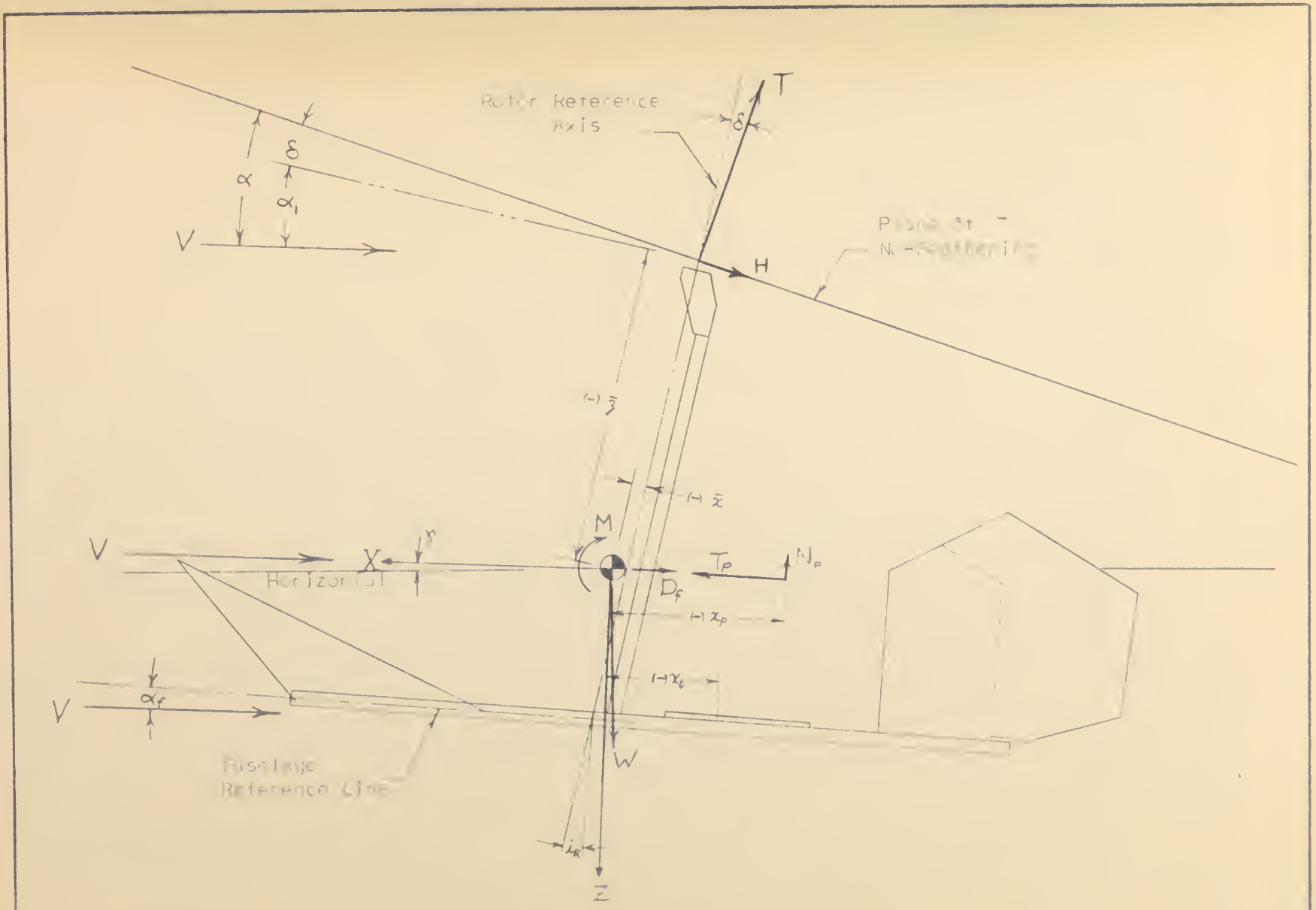
Rotor Reference Axis
T
δ
ε
α
α_1
V
H
Plane of No-Feathering
$(-)\bar{z}$
$(-)\bar{x}$
M
V
X
r
Horizontal
T_p
N_p
D_f
$(-)x_p$
$(-)x_t$
V
α_f
Fuselage Reference Line
W
i_R
$\bar{z}$

FIGURE 2

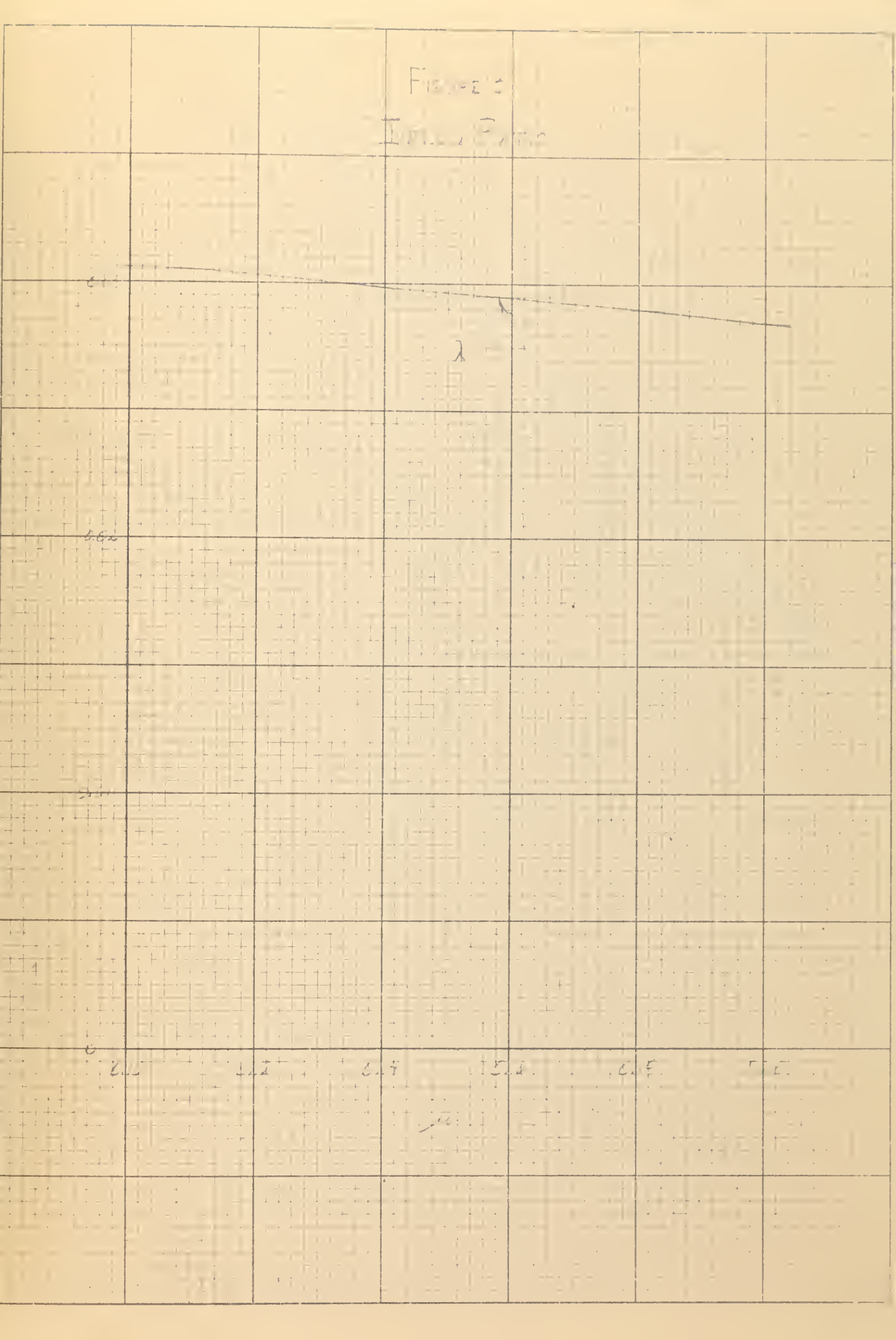
λ

FIGURE 4

RATE SPEED - VELOCITY DERIVATIVE

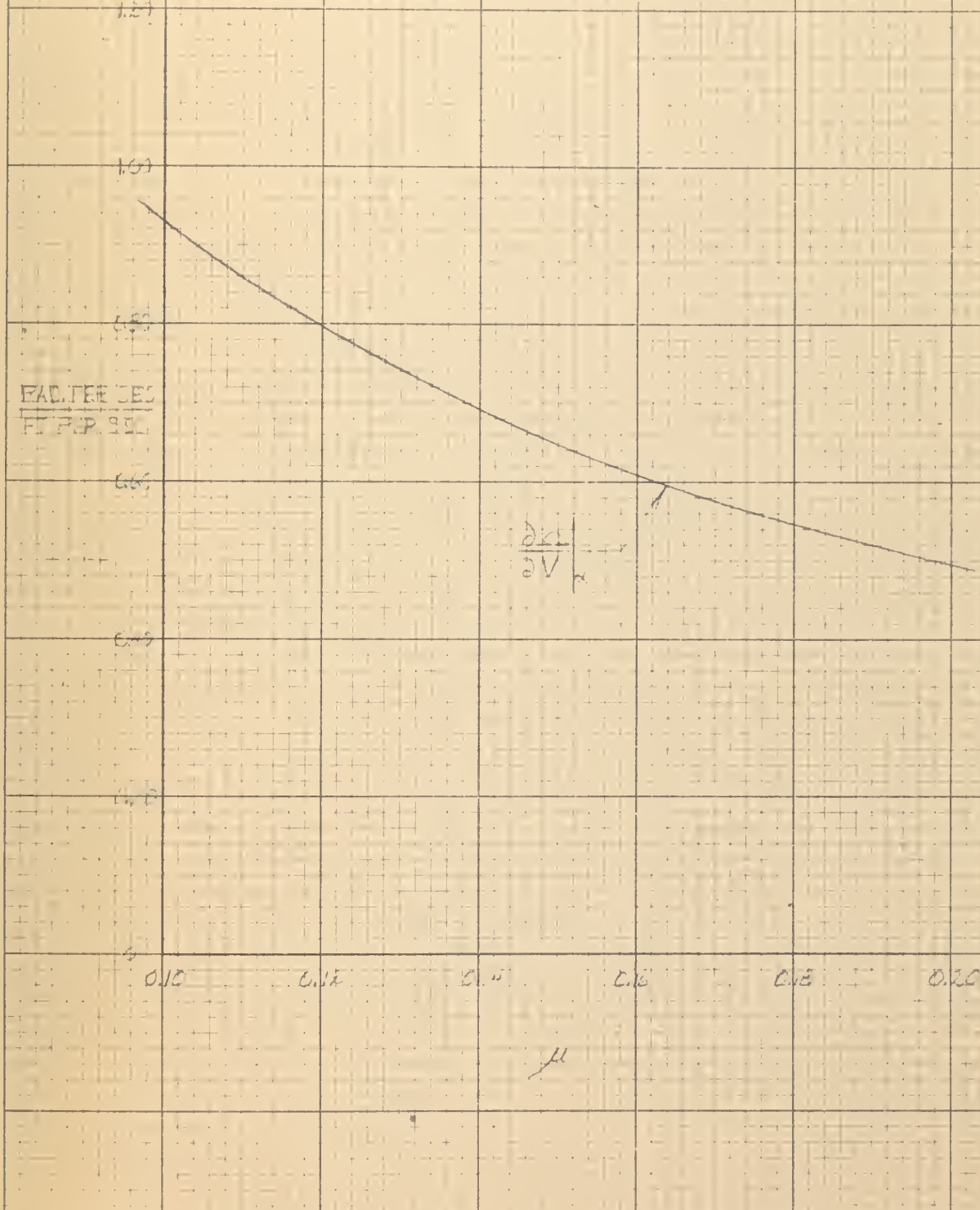

FACILITIES
FT P.P. 92

FIGURE 5

ROTOR SPEED - ANGLE OF ATTACK DERIVATIVE

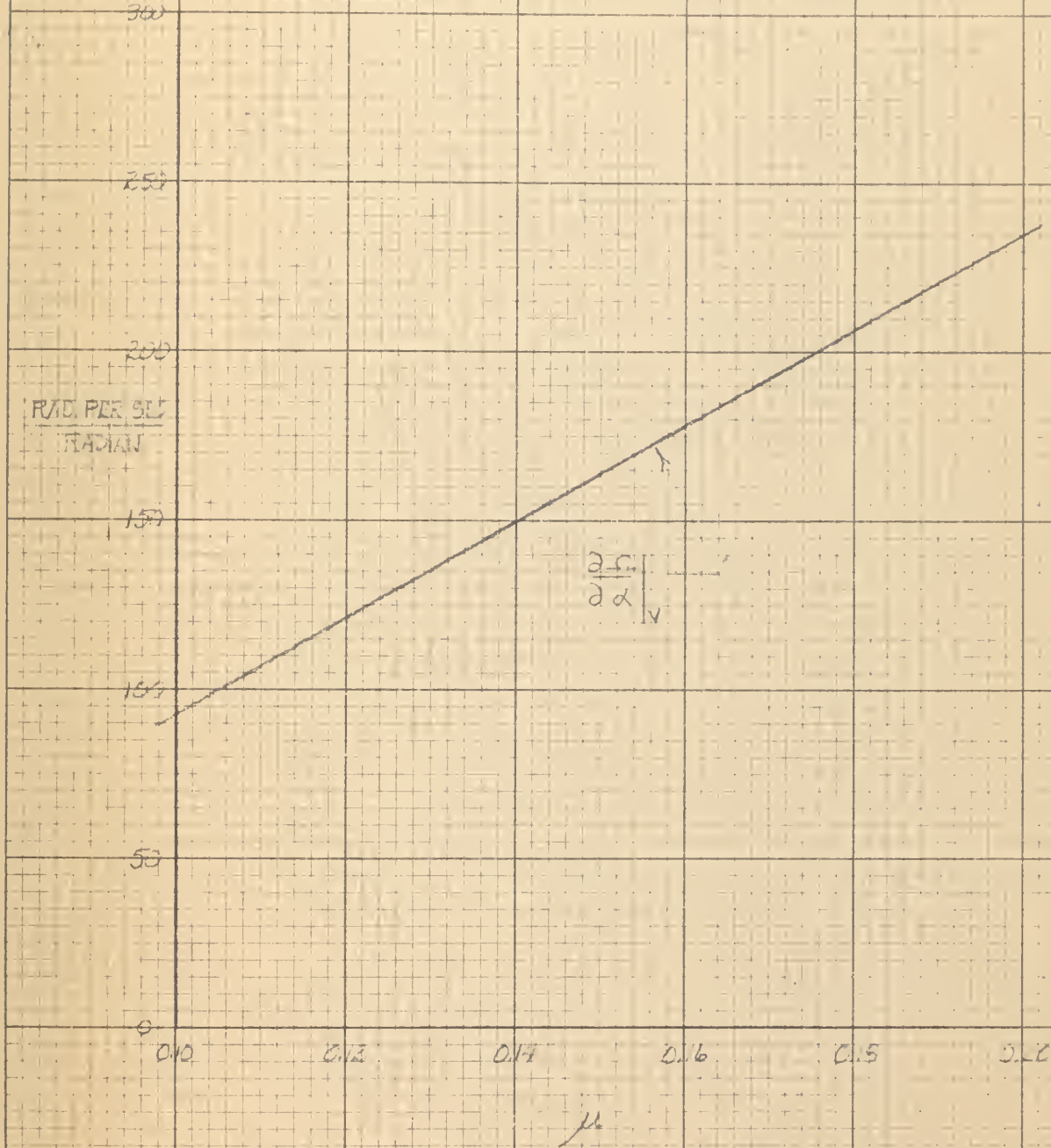

FIGURE 6

ROTOR THRUST - VELOCITY DERIVATIVE

$-Z_v$

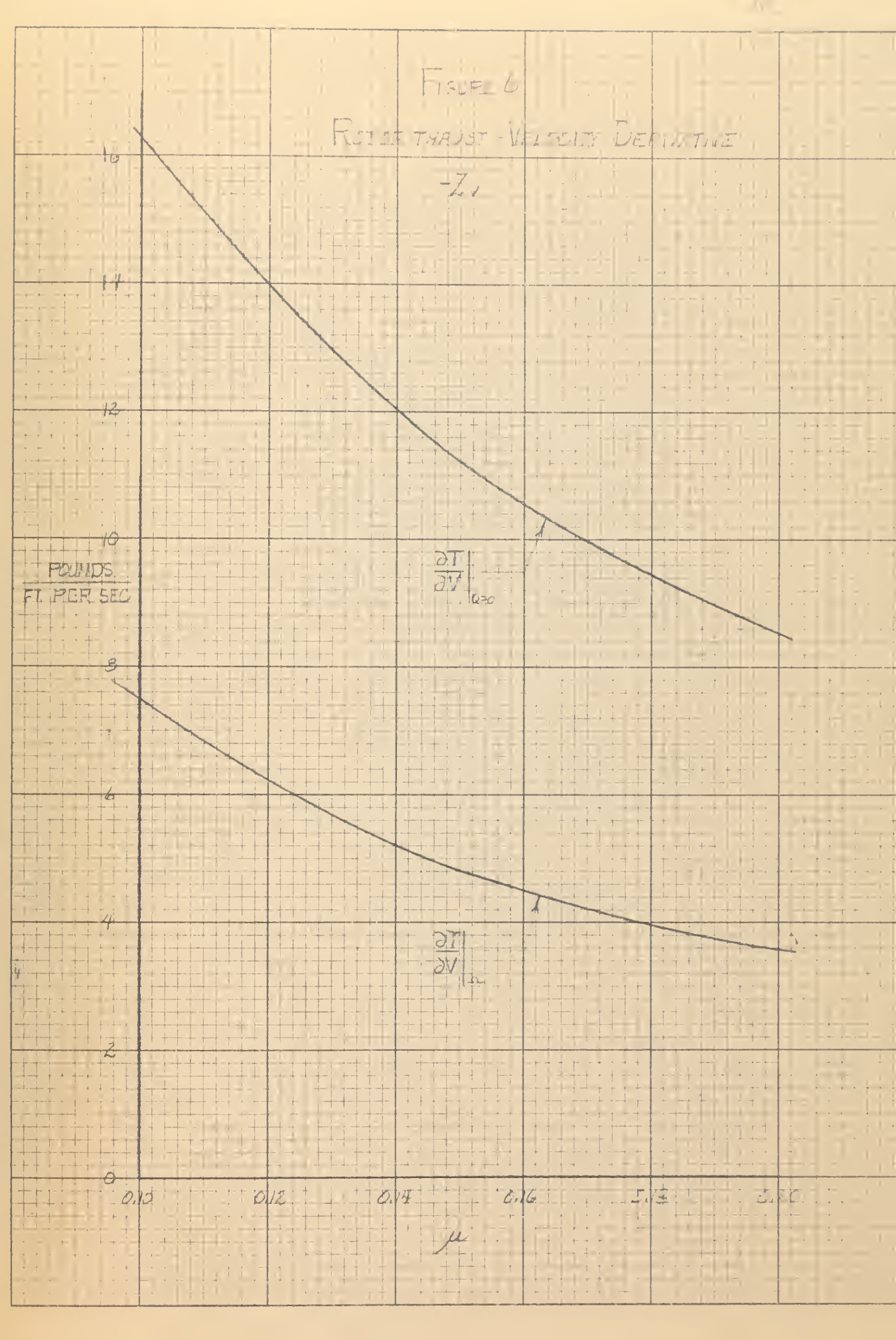

FIGURE 7

PEECE THRUST ANGLE OF ATTACK DERIVATIVE

$-Z_\alpha$

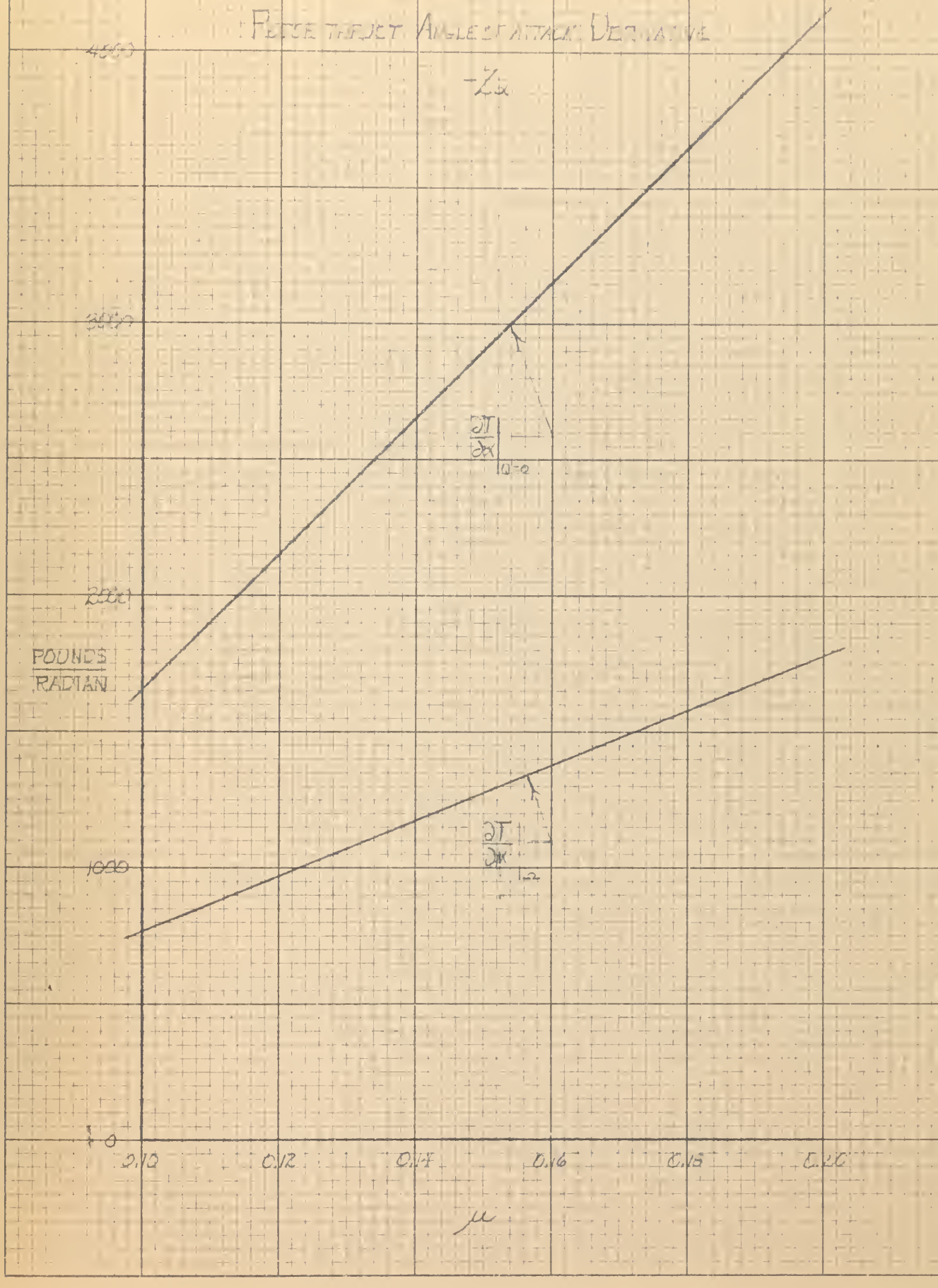

FIGURE 8

POTOCKI FORCE COEFFICIENTS

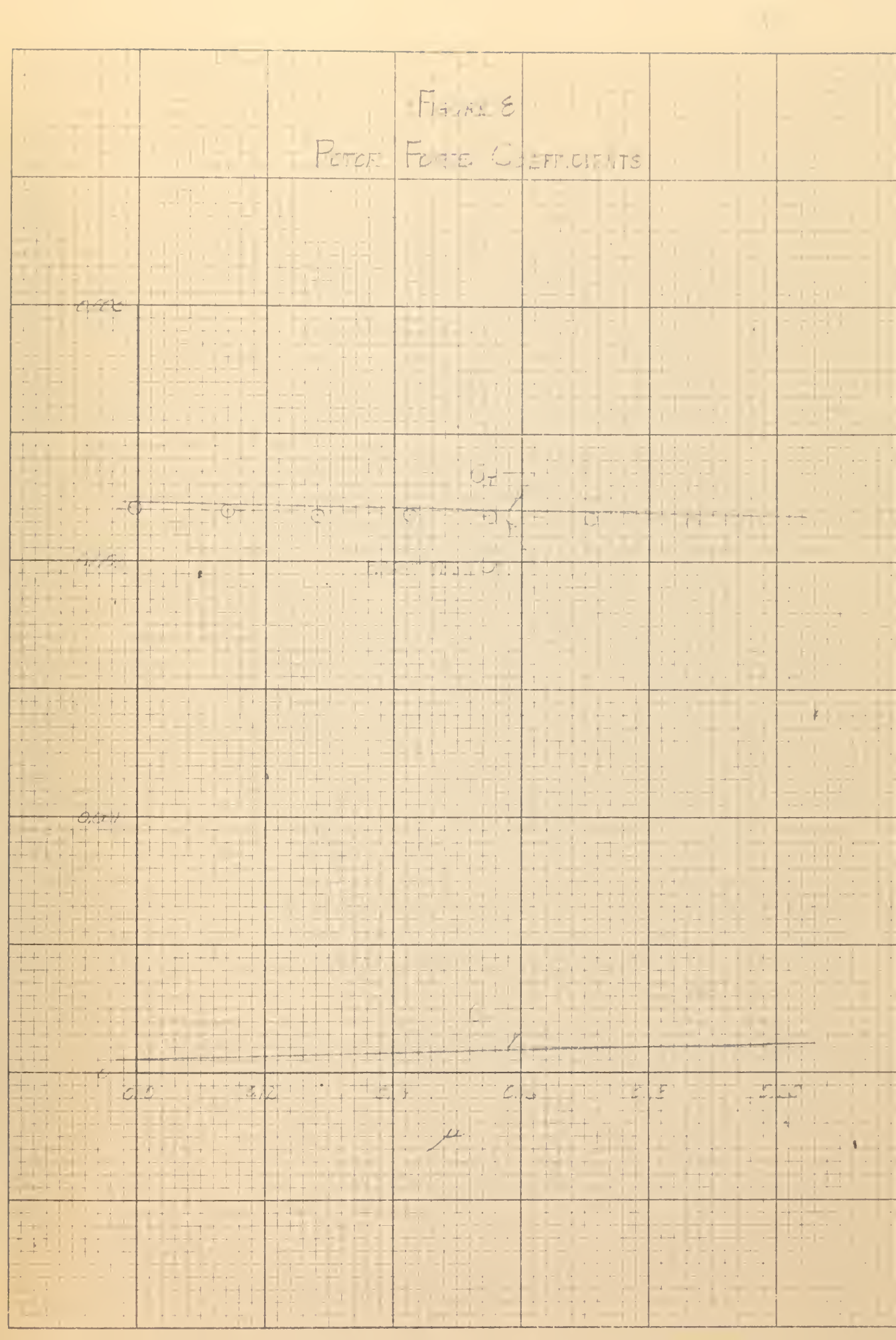

FIGURE 9

FILTER H FIELD

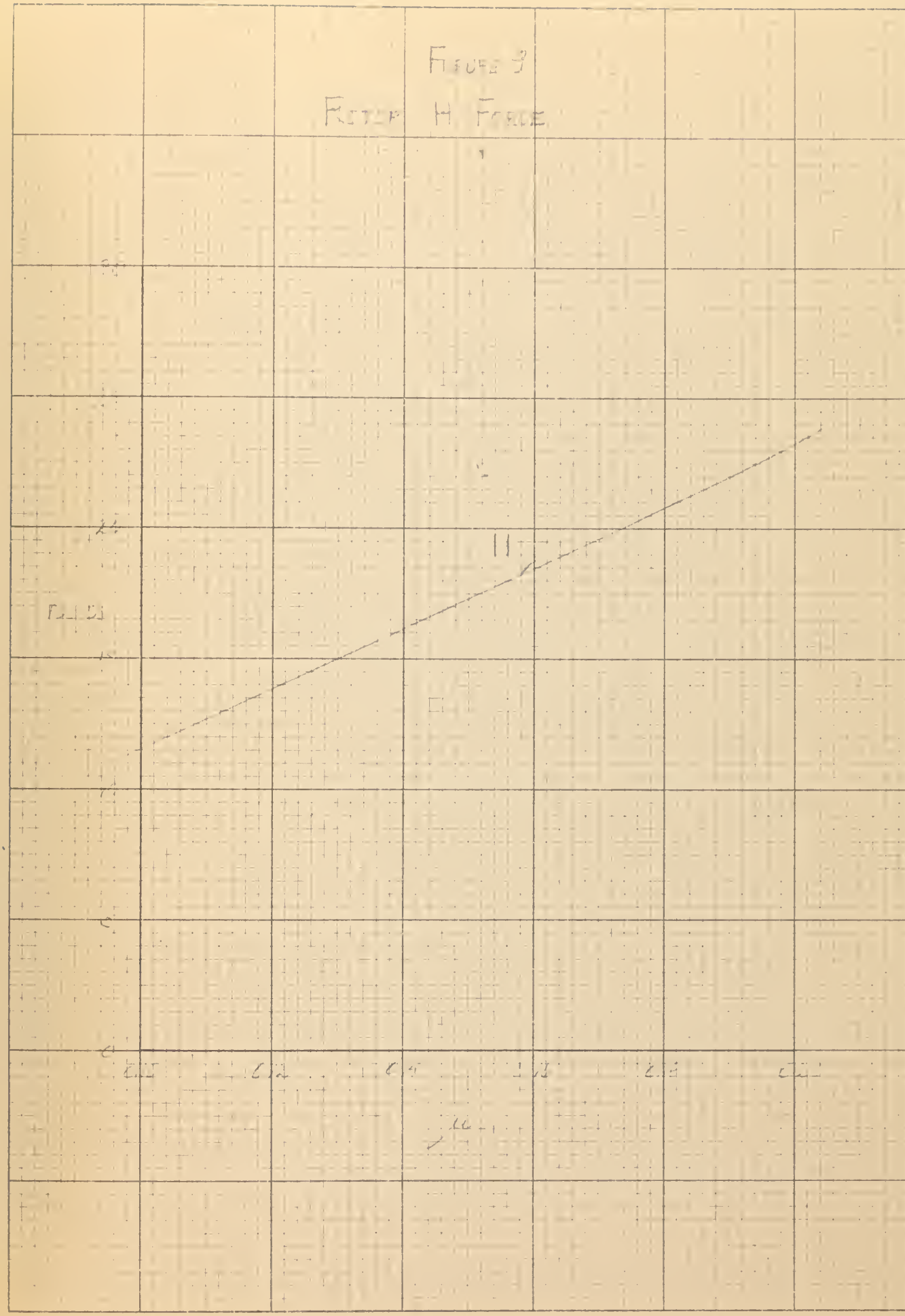

FIGURE 12

H FORCE - VELOCITY DERIVATIVE

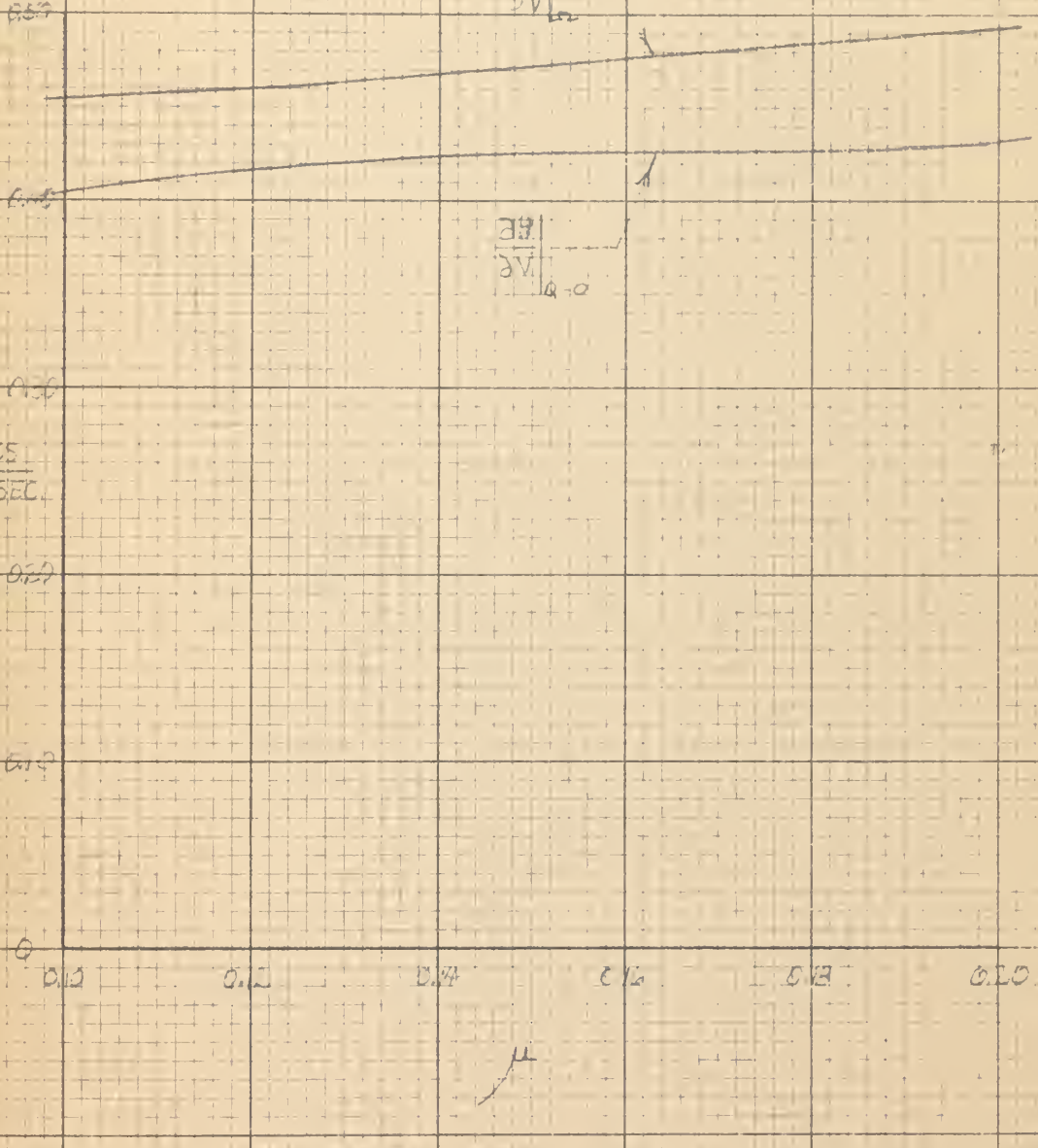

FIGURE 1

H FORCE - ANGLE OF ATTACK DERIVATIVE

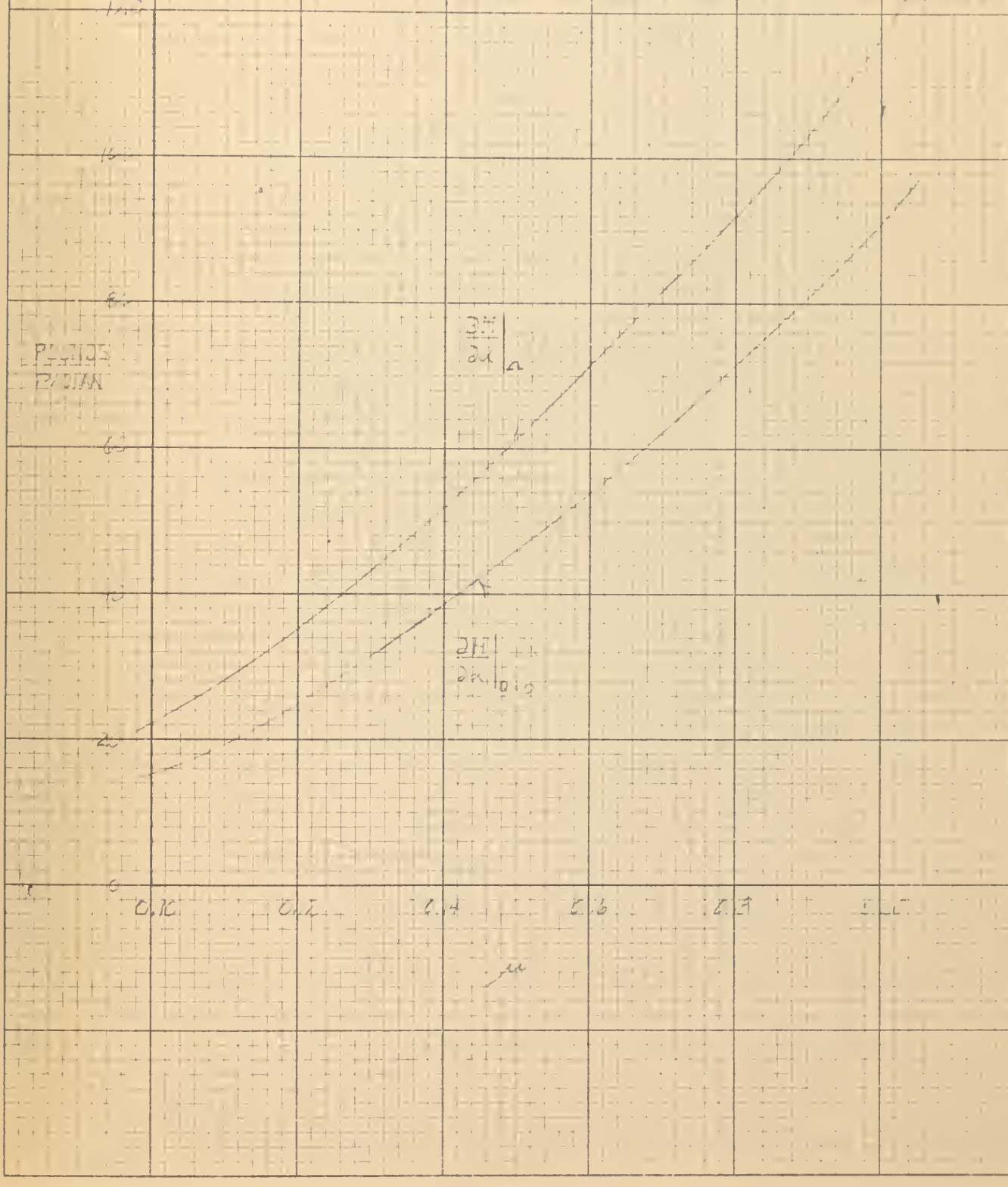

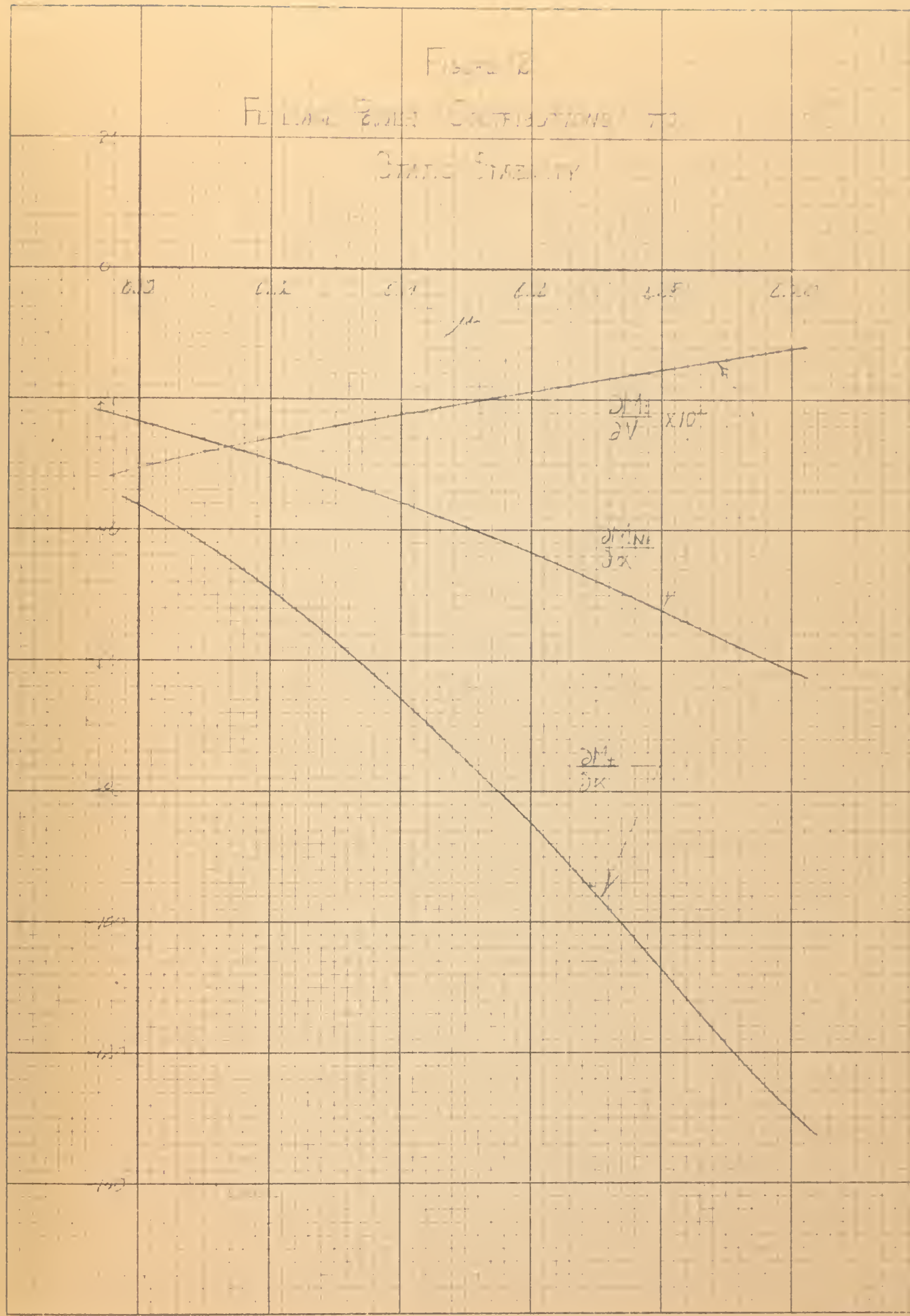
$\frac{\partial C_{M_{ac}}}{\partial V} \times 10^{-2}$
$\frac{\partial C_{M_{ac}}}{\partial \alpha}$
$\frac{\partial C_{M_{ac}}}{\partial \alpha}$

FIGURE 15

ROTOR VELOCITY STABILITY

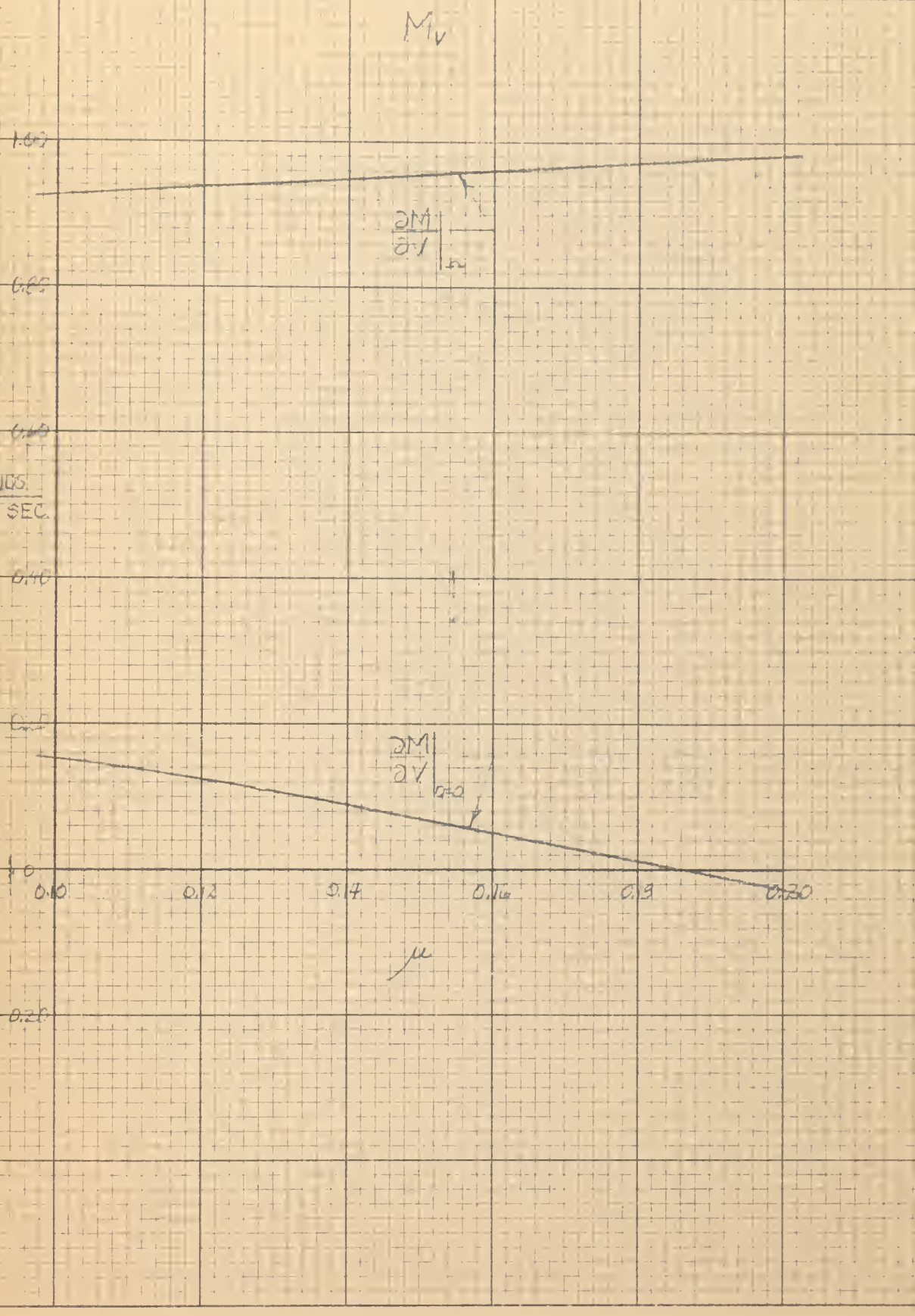

FIGURE 17

FORCE AND STABILITY

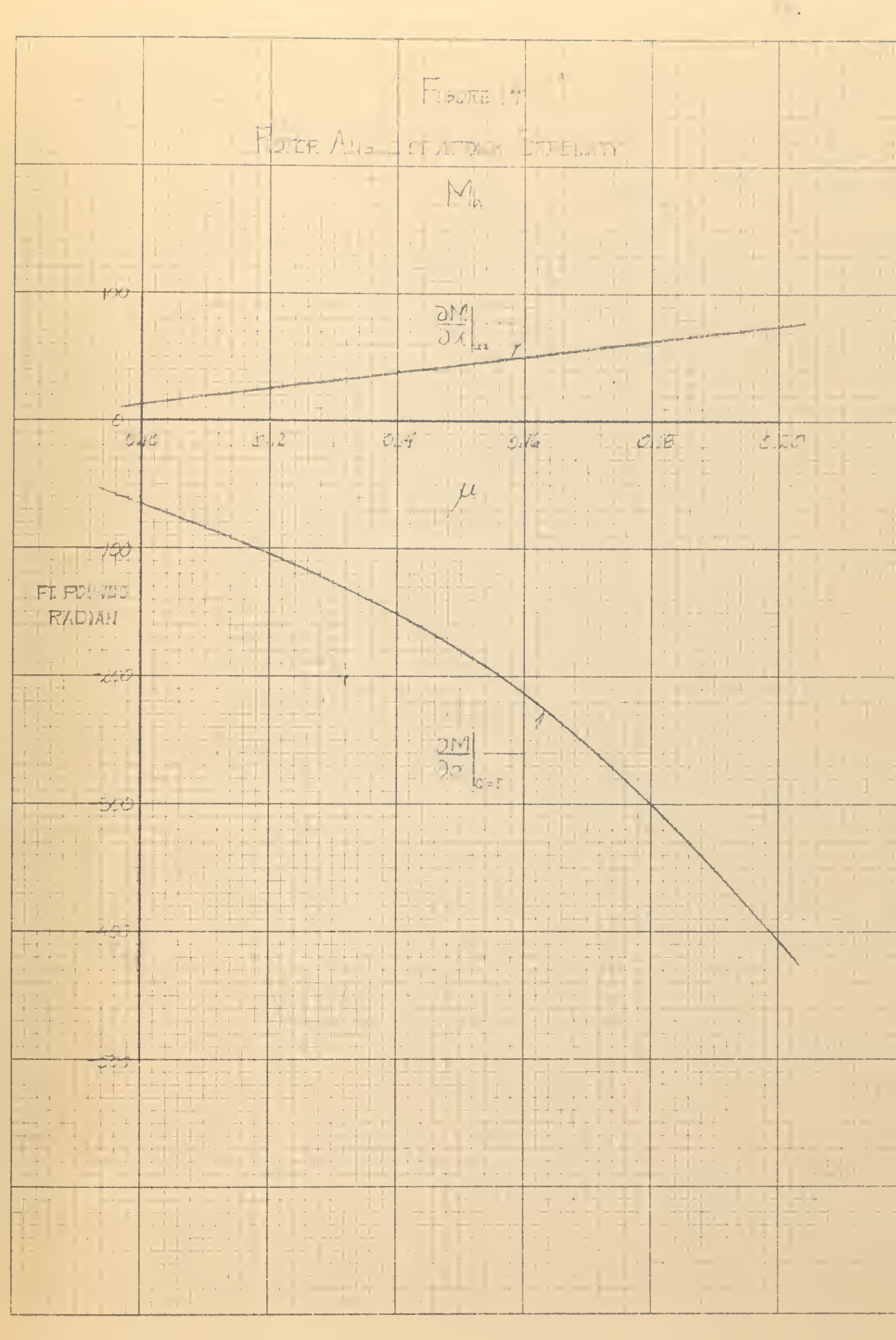

FIGURE 15

AIRPLANE VELOCITY STABILITY

M_{1V}

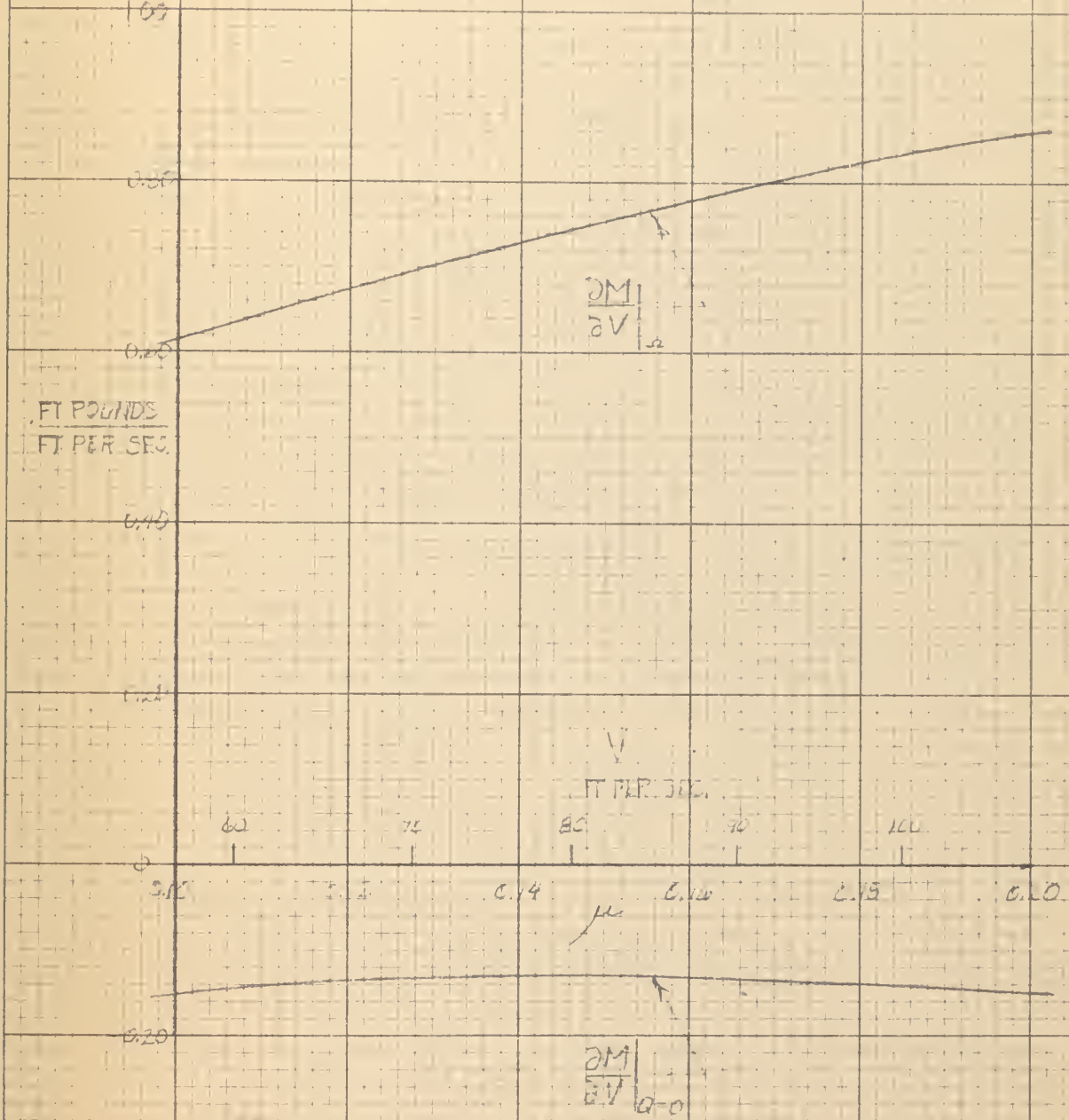

FIGURE 16

AIRCRAFT ANGLE OF ATTACK STABILITY

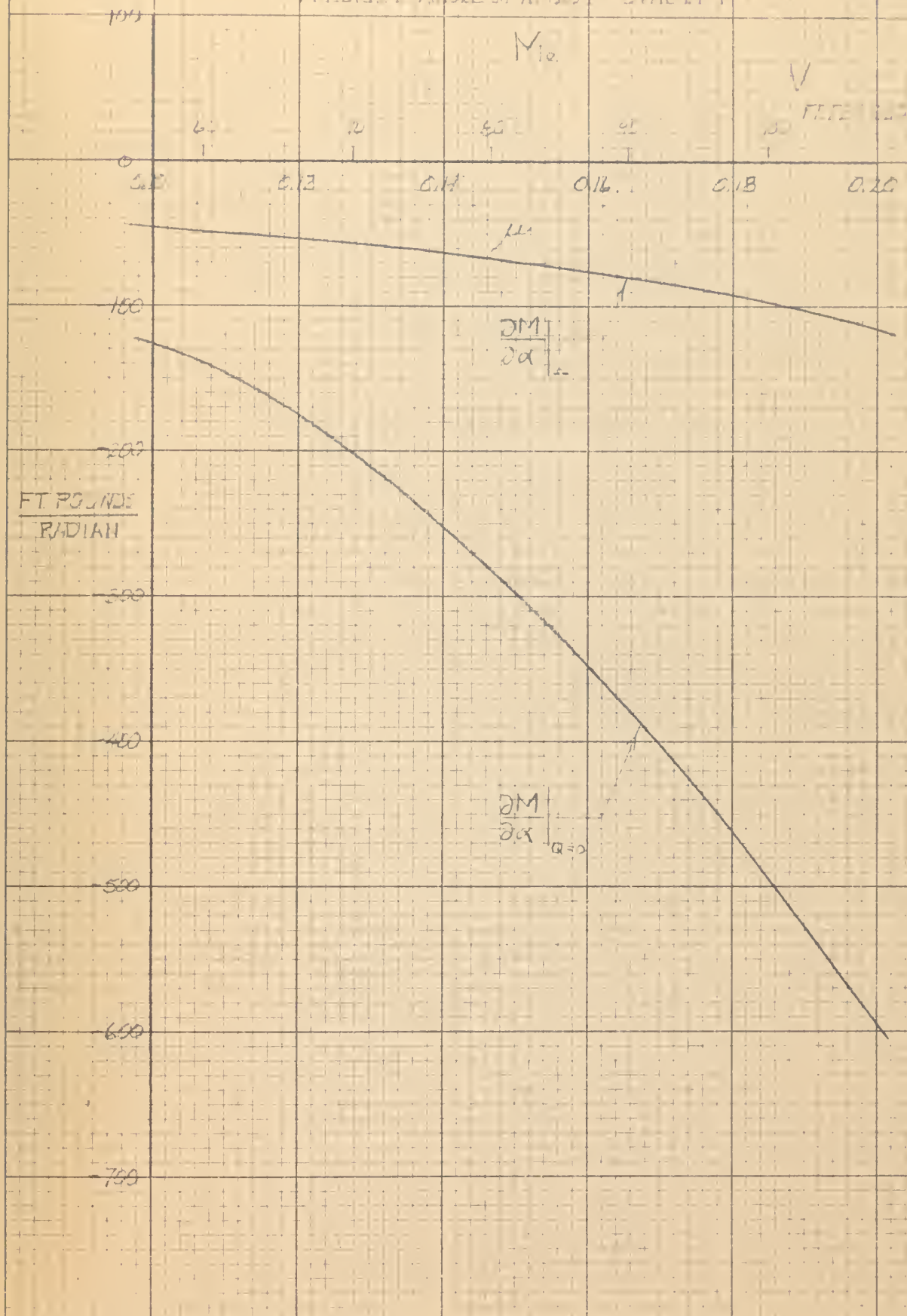

FIGURE 11

AIRCRAFT CONTROL MOMENT

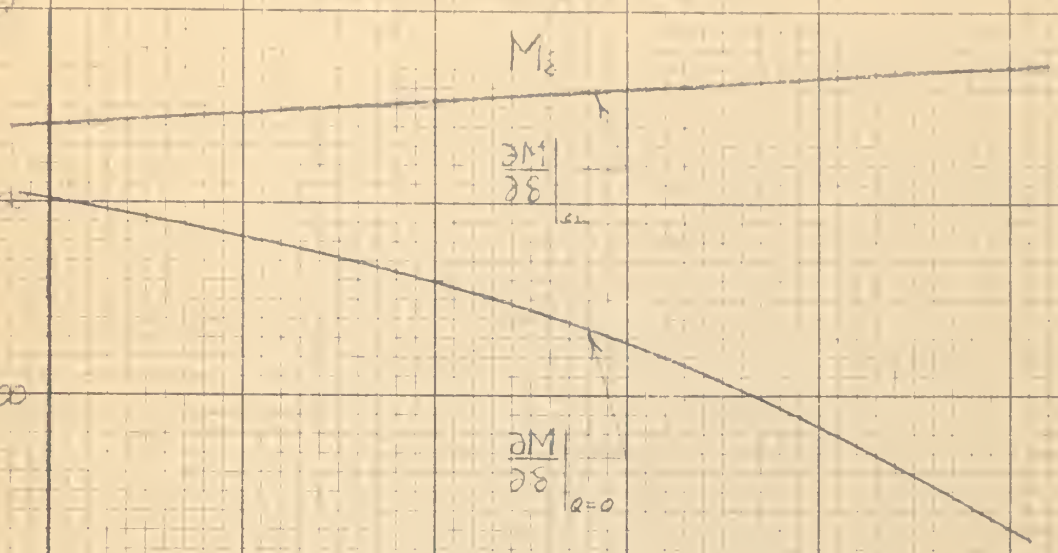

FT. POUNDS PER RADIAN

1400
1200
1000
800
600
400
200
0

V
FT PER SEC

40
60
80
100
120

0.10
0.12
0.14
0.16
0.18
0.20

μ

FIGURE 16

ARRESTED CALIBRATION

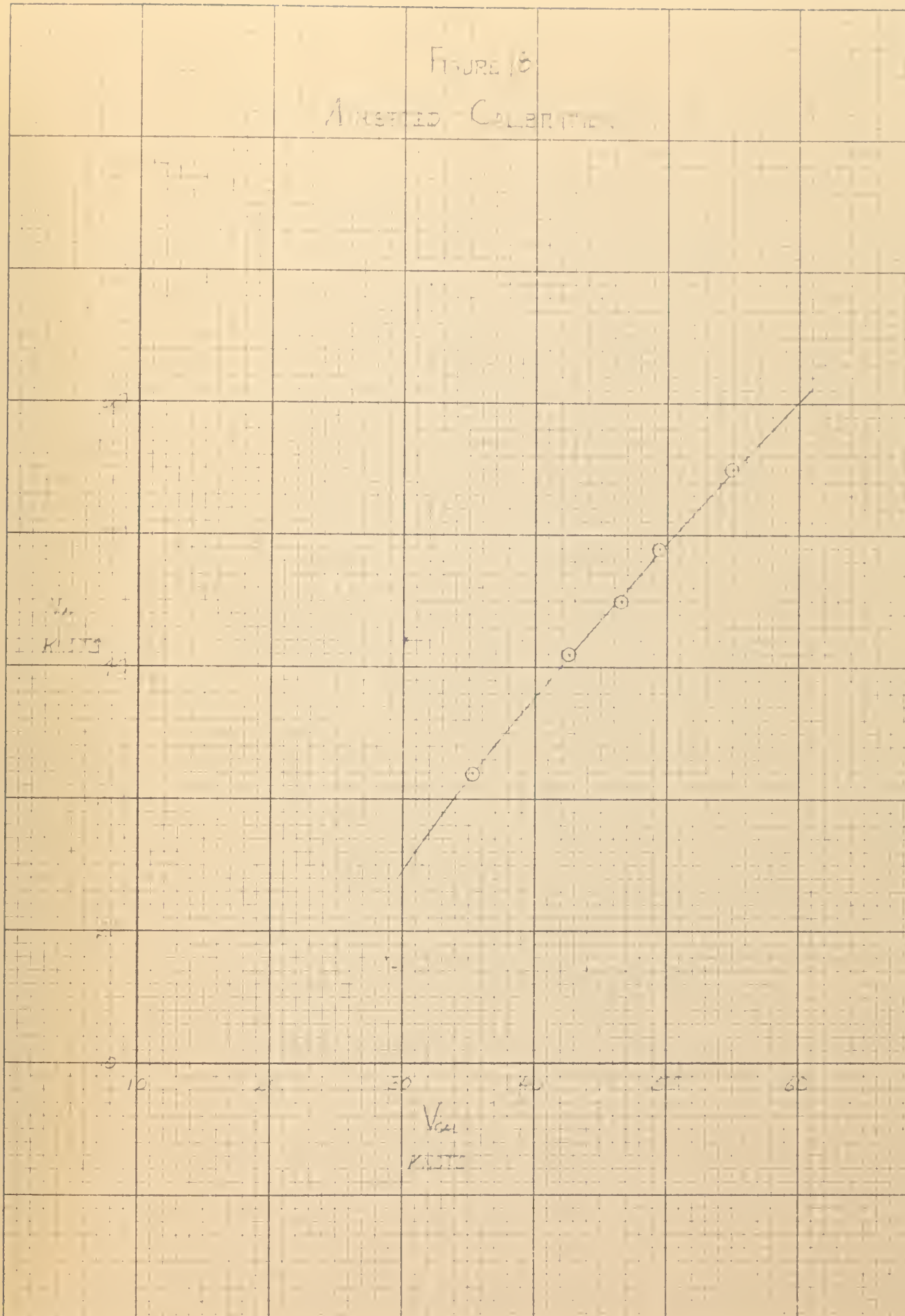

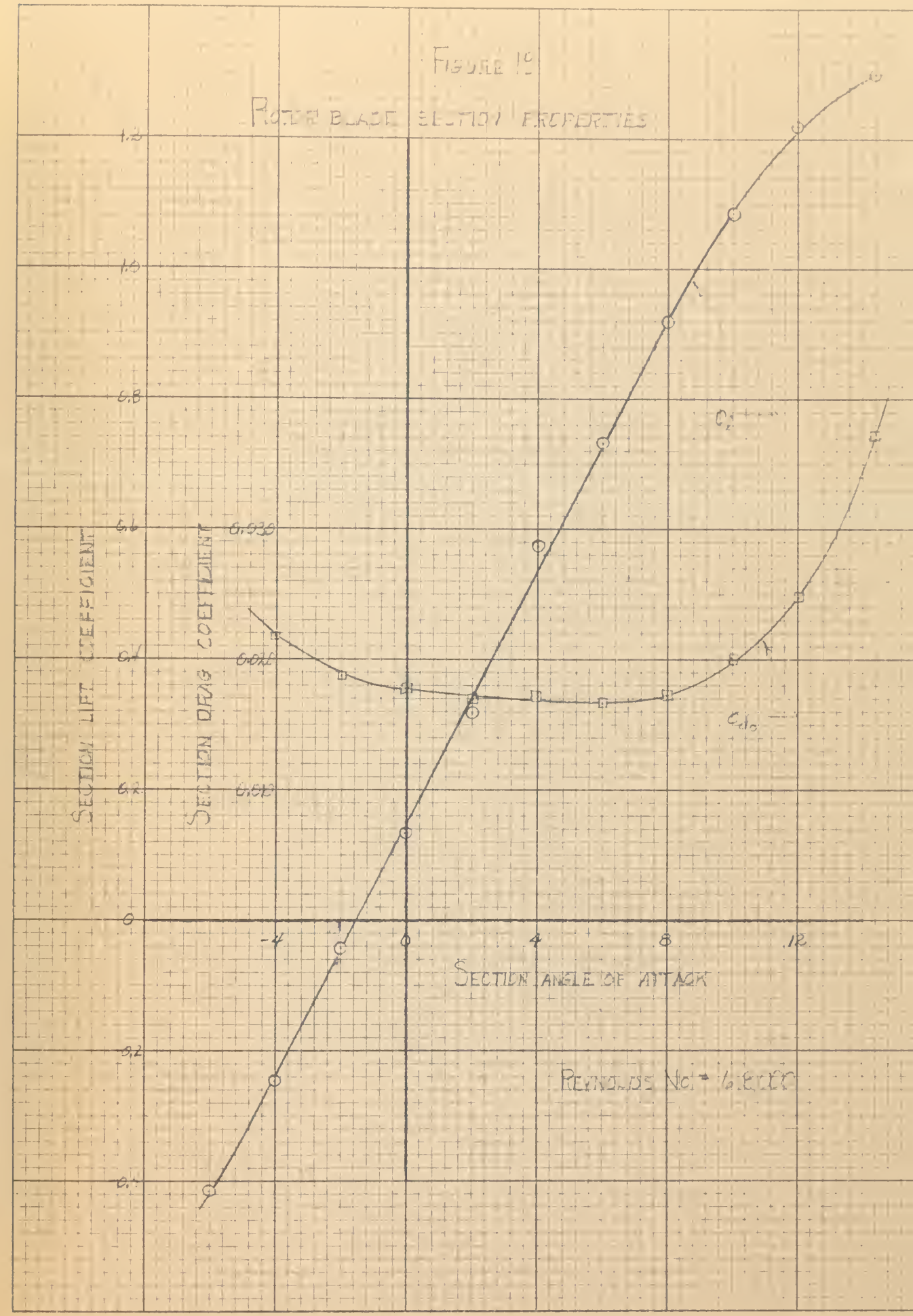
FIGURE 10
ROTOR BLADE SECTION PROPERTIES
1.2
1.0
0.8
0.6
0.4
0.2
0
0.2
SECTION LIFT COEFFICIENT
SECTION DRAG COEFFICIENT
0.030
0.020
0.010
-4
0
4
8
12
SECTION ANGLE OF ATTACK
C_l
C_{d_0}
REYNOLDS NO. = 6.8 E6

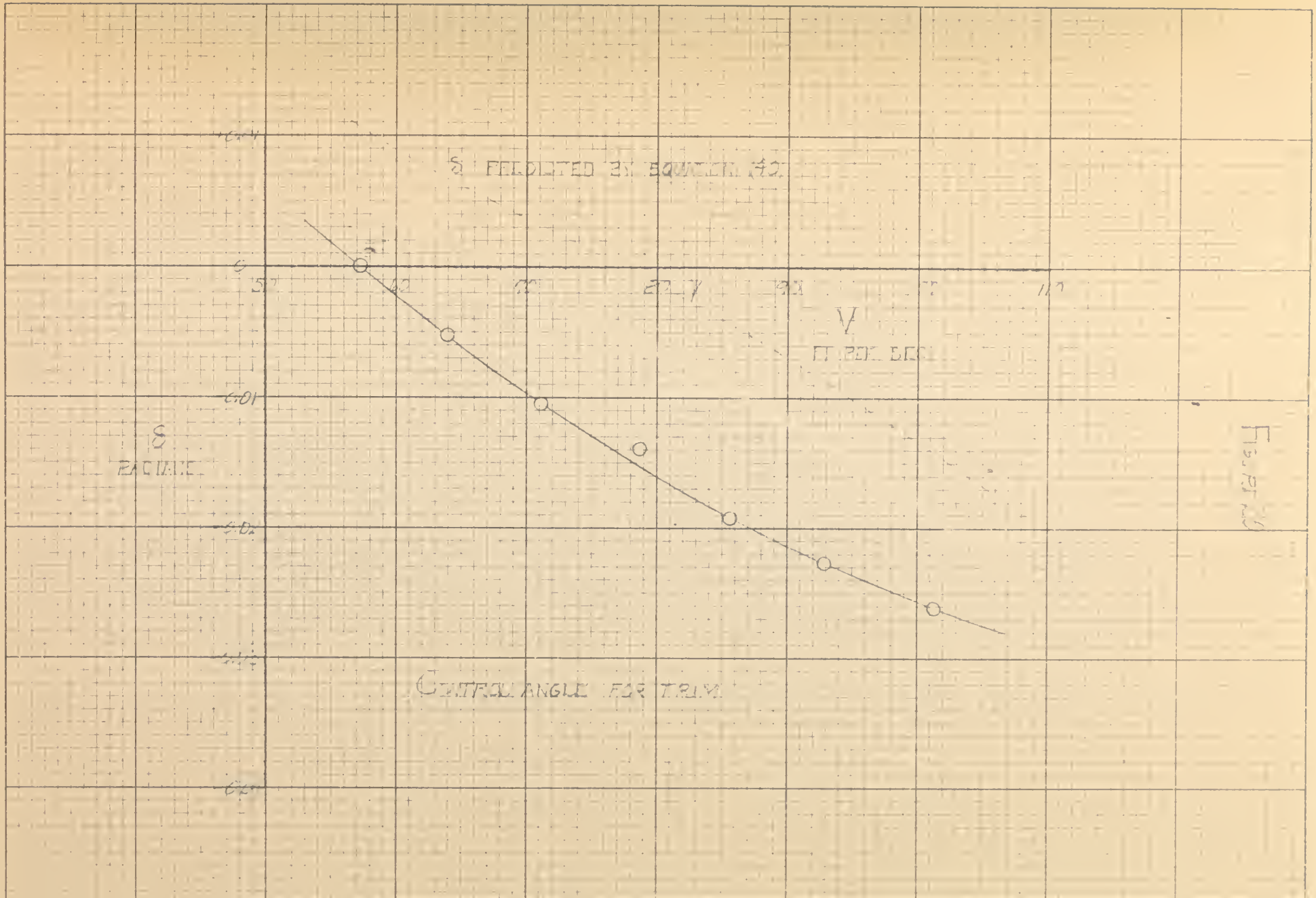
δ PLOTTED BY EQUATION 40
V
FT PER SEC
δ
RADIANS
CONTROL ANGLE FOR TRIM

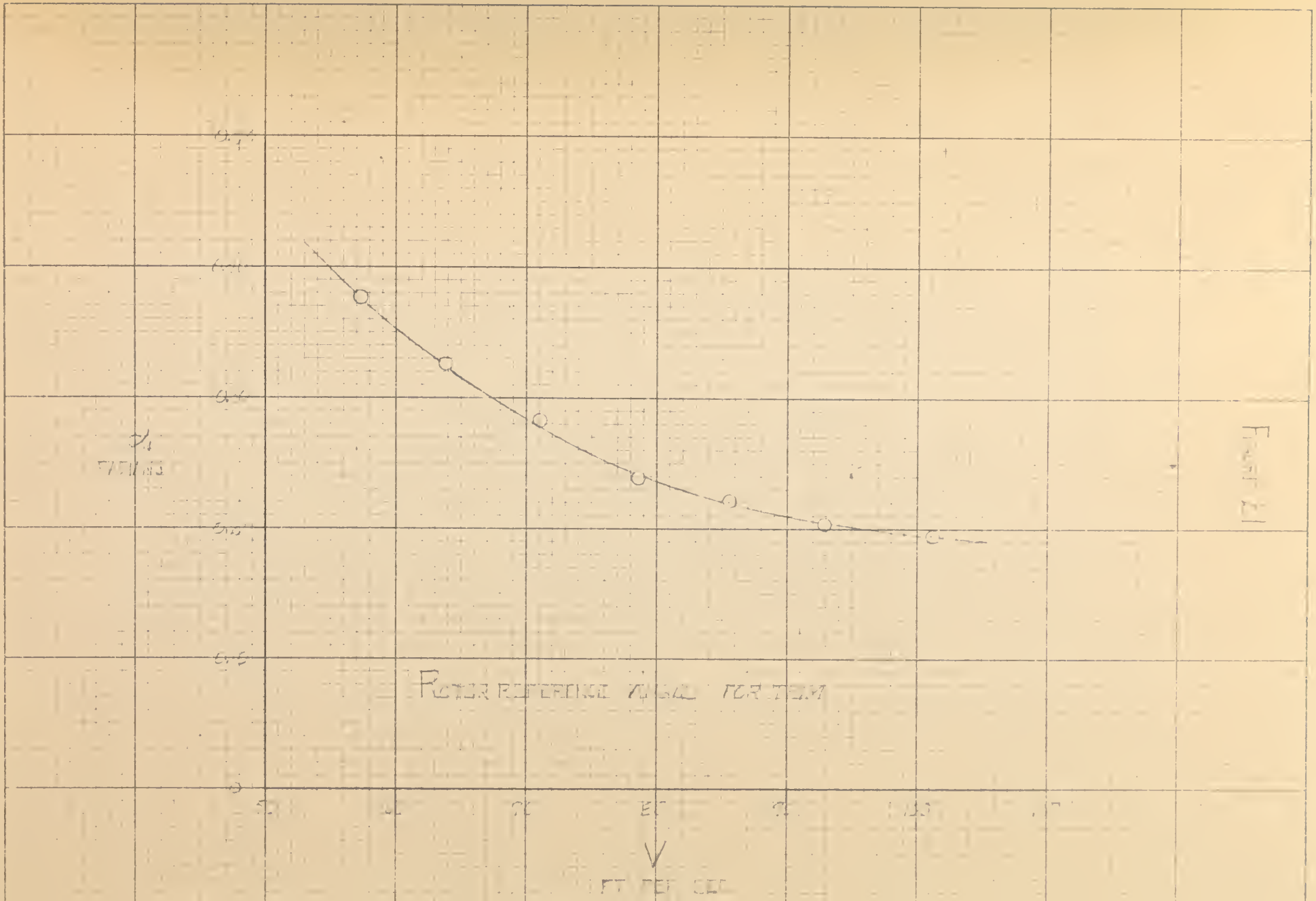

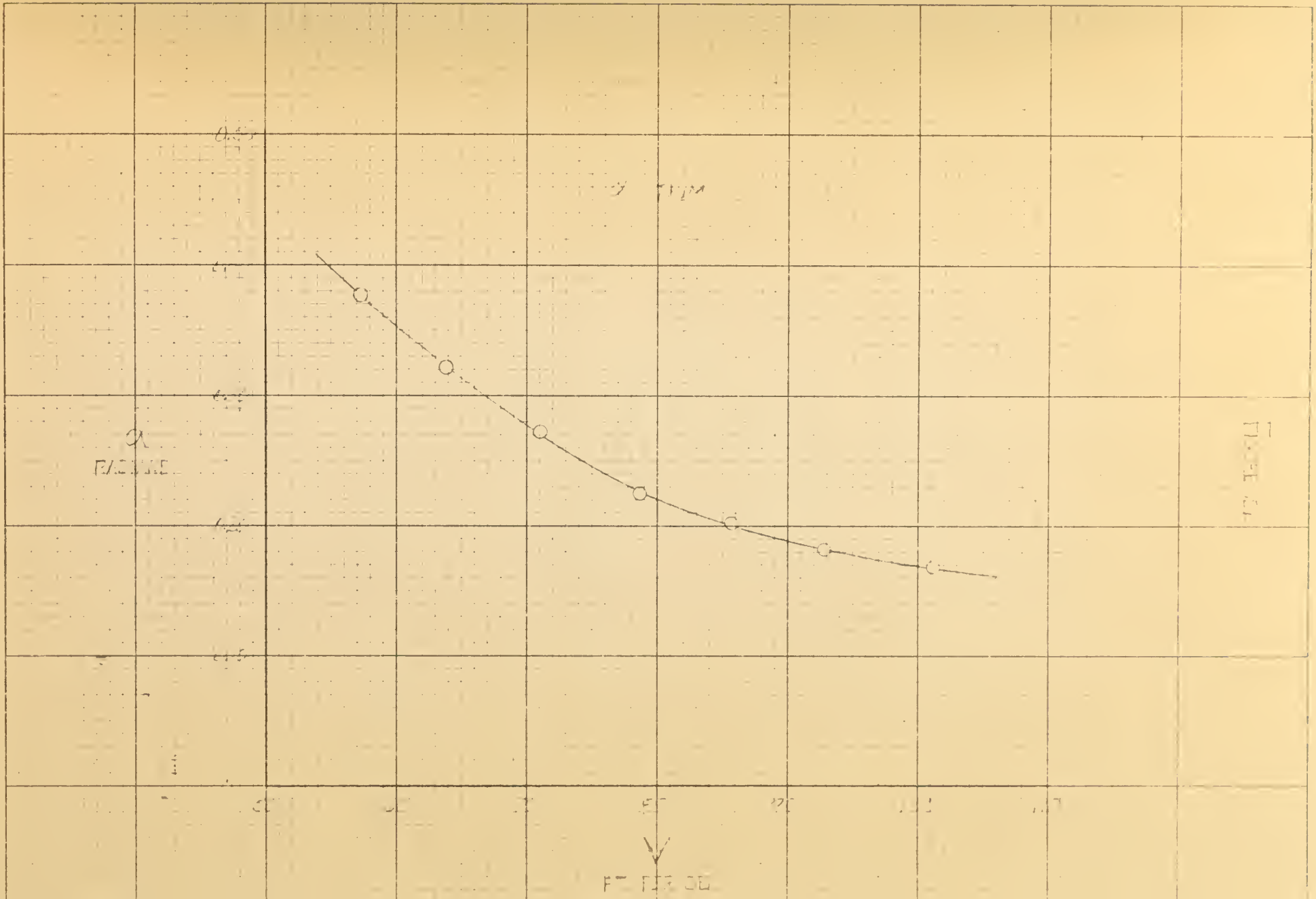

FIGURE 6.

STATIC STABILITY

$E = \frac{1}{2}[\sum_{i=1}^{n} A_i M_i - \sum_{i=1}^{n} A_i M_i]$

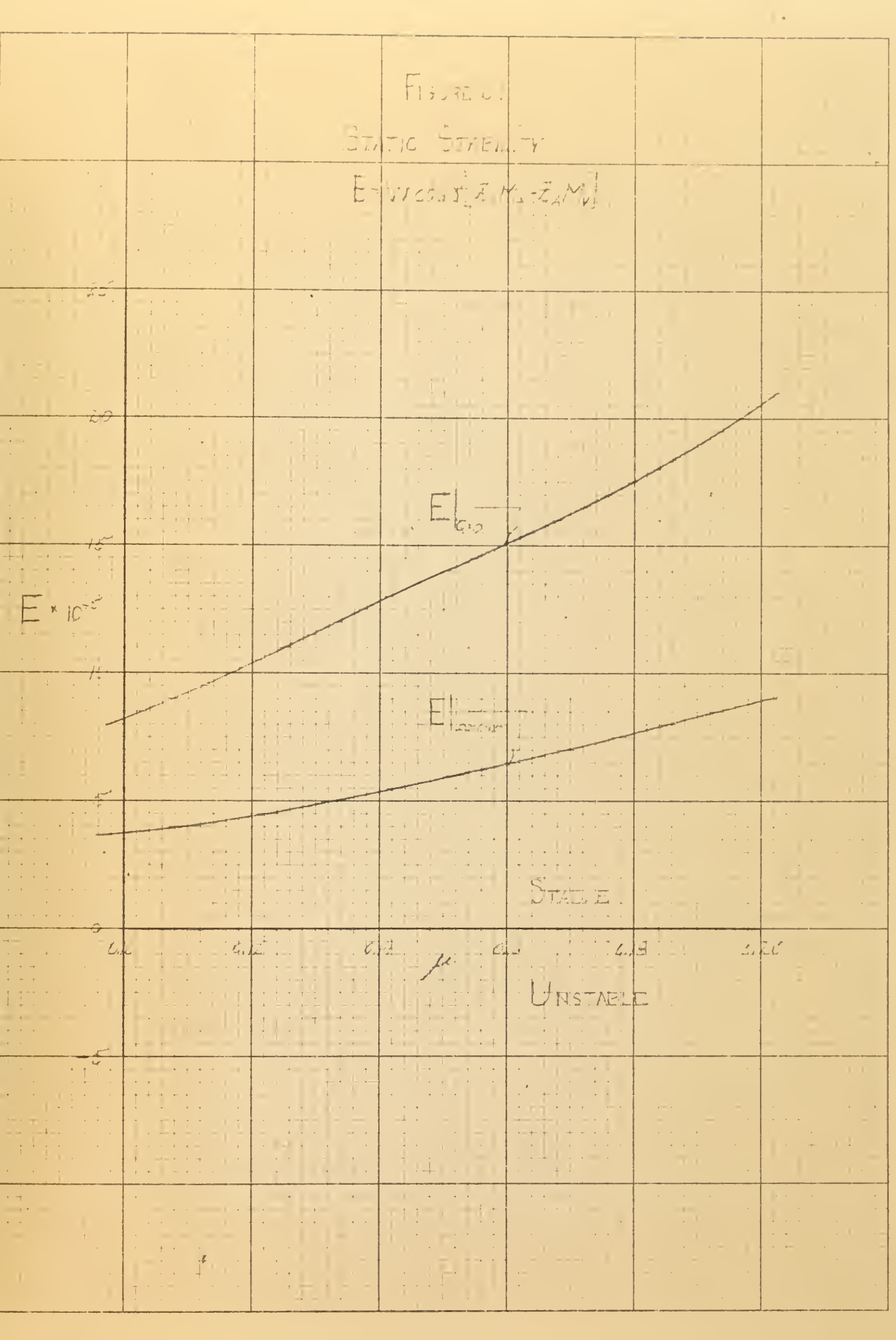

APPENDIX I

Physical Constants for Bensen B-8M Autogyro

Gross weight	$W = 4[illegible]$ lb.
Center of gravity in relation to rotor reference axis	$\bar{x} = -0.10[illegible]$ ft.
	$\bar{z} = -[illegible]$ ft.
Equivalent flat plate drag area, fuselage (estimated)	$f = 8$ ft^2
Engine - 4 cyl. McCulloch 4318-A	72 HP @ 4100 RPM (rated)
Thrust axis parallel to fuselage reference axis ($\alpha_p = \alpha_f$)	$x_p = -2.[illegible]$ ft
	$z_p = +0.004[illegible]$ ft.
Propeller - 45-24 Bank-Maxwell two-bladed pusher	
Horizontal tail - Area	$S_t = 2.[illegible]$ ft^2
Aspect ratio	$A = 1.[illegible]4$
Lift curve slope	$a_t = 2.0$
Sweep of quarter chord	$\Lambda = 4[illegible]^\circ$
Tail arm	$x_t = -1.[illegible]2$ ft
Tail incidence	$i_t = 0$
Rotor (teeter hinge)	
Number of blades	$b = 2$
Radius of blade	$R = 10$ ft
Blade chord (constant)	$c = 0.[illegible]$ ft
Rotor solidity	$\sigma = 0.0358$
Built-in coning angle	$\beta_0 = 0.07$ radians
Blade pitch angle	$\theta_0 = 0.0262$ radians
Blade twist	$\theta_1 = 0$
Blade airfoil section	Bensen G-3
Lift curve slope	$a = 5.[illegible]$ per radian
Drag coefficient as a power series	$C_{d_0} = \delta_0 + \delta_1 r + \delta_2 r^2$
	$\delta_0 = 0.01[illegible]$
	$\delta_1 = -0.0[illegible]09$
	$\delta_2 = 0.3170$
Mean drag coefficient	$\bar{\delta} = 0.01[illegible]$
Mass moment of inertia about the flapping hinge (per blade)	$I_\beta = 20.77$ slug ft^2
Mass moment about flapping hinge (per blade)	$M_g = 2.87$ slug ft^2
Weight moment about flapping hinge (per blade)	$M_W = 92.[illegible]$ lb ft
Lock's blade constant $\gamma_l = \frac{\rho a c R^4}{I_\beta}$	$\gamma_l = 3.[illegible]4$
Incidence of plane perpendicular to rotor reference axis to fuselage reference line	$i_R = 3.7^\circ$

APPENDIX II

Aerodynamic Torque Relations

Bailey, in Ref. 4, gives the following relations for the accelerating and decelerating torque acting on a lifting rotor having no blade twist: (neglecting terms of the order μ^3 and higher)

1. Accelerating Torque:

$$\frac{2C_Q}{\sigma} = a(t_{4,1})\lambda^2 + a(t_{4,2})\lambda\theta_o + a(t_{4,4})\theta_o^2$$

where

$$t_{4,1} = \frac{B^2}{2} + \left(\frac{5}{4} - \frac{\gamma_1^2 B^8}{1296}\right)\mu^2$$

$$t_{4,2} = \frac{B^3}{3} + \left(\frac{8B}{3} + \frac{\gamma_1^2 B^9}{864}\right)\mu^2$$

$$t_{4,4} = \left(\frac{8B^2}{9} + \frac{\gamma_1^2 B^{10}}{1080}\right)\mu^2$$

2. Decelerating Torque:

$$\frac{2C_Q}{\sigma} = \delta_o(t_{5,1}) + \delta_1[(t_{5,2})\lambda + (t_{5,3})\theta_o] + \delta_2[(t_{5,5})\lambda^2 + (t_{5,6})\theta_o + (t_{5,8})\theta_o^2]$$

where

$$t_{5,1} = \frac{1}{4} + \frac{1}{4}\mu^2$$

$$t_{5,2} = \frac{1}{3}$$

$$t_{5,3} = \frac{1}{4} + \frac{1}{4}\mu^2$$

$$t_{5,5} = \frac{1}{2} + \left(-\frac{1}{4} + \frac{1}{B^2} + \frac{1}{2B^4} + \gamma_1^2\left(\frac{B^4}{162} - \frac{B^5}{81} + \frac{B^6}{144}\right)\right)\mu^2$$

$$t_{5,6} = \frac{2}{3} + \left(\frac{4}{3B} + \frac{4}{3B^3} + \gamma_1^2\left(\frac{B^5}{108} - \frac{B^6}{54} + \frac{B^7}{96}\right)\right)\mu^2$$

$$t_{,3} = \frac{1}{4} + \left[\frac{1}{4} \quad \frac{8}{9B^2} + \gamma_1^2 \left(\frac{B^6}{288} - \frac{B^7}{144} + \frac{B^8}{256} \right) \right] \mu^2$$

Using a tip loss factor $B = 1 - \frac{c}{2R} = 0.972$, substituting the known rotor characteristics as listed in Appendix I into the above equations, and again, the accelerating to decelerating torque yields the following expression for the total aerodynamic torque:

$$C_Q = \frac{\sigma}{2} \left[\mu^2(A_1\lambda^2 + A_2\lambda + A_3) - (B_1\lambda^2 + B_2\lambda + B_3) \right]$$

where

$A_1 = 0.471$
$A_2 = 0.3504$
$A_3 = -0.001144$
$B_1 = -2.429250$
$B_2 = -0.025330$
$B_3 = 0.004121$

At an equilibrium rotor speed, the torque is zero.

$$C_Q = 0$$

and

$$\mu^2 = \frac{B_1\lambda^2 + B_2\lambda + B_3}{A_1\lambda^2 + A_2\lambda + A_3}$$

For a given tip speed ratio the above relation results in a quadratic in inflow ratio. The larger arithmetic value obtained from the solution of the quadratic corresponds to rotor operation at a positive angle of attack.

thesC478
An investigation of the longitudinal sta
3 2768 002 10416 8
DUDLEY KNOX LIBRARY